

Surface forcing on the southern flank of Georges Bank, February–August 1995

Robert C. Beardsley, Steven J. Lentz, Robert A. Weller, Richard Limeburner, James D. Irish, and James B. Edson

Woods Hole Oceanographic Institution, Woods Hole, Massachusetts, USA

Received 22 February 2002; revised 19 February 2003; accepted 2 April 2003; published 10 October 2003.

[1] Surface wind stress, heat, and freshwater fluxes were estimated over the southern flank of Georges Bank during February–August 1995 using moored measurements made at ST1 located on the 76-m isobath, roughly halfway between the tidal mixing and shelf/slope fronts. Wind stress variability was dominated by a succession of atmospheric lows that passed Georges Bank during the deployment. A transition between frequent lows and strong wind stress events (“winter”) to less frequent lows and weaker wind stresses (“summer”) occurred in mid-May. In winter, wind stress fluctuations tended to be omnidirectional, with maximum stresses above 0.5 N/m^2 during four storms, one a classic “nor’easter”, while summer fluctuations were weaker but strongly polarized in the along-bank direction. The ST1 surface heat flux was dominated by shortwave heating, which increased from a winter mean of 130 W/m^2 to 230 W/m^2 in summer. Long-wave cooling decreased from 50 W/m^2 (winter) to 30 W/m^2 (summer), while mean sensible and latent fluxes increased from -20 and -40 W/m^2 (winter) to $+10$ and 0 (summer) respectively. Overall, winter was characterized by weak net heating (30 W/m^2) with shortwave gain offset by long-wave, latent, and sensible heat loss. In summer, increased shortwave gain and reduced long-wave loss and weak sensible and latent fluxes combined to produce strong net heating (210 W/m^2). ST1 precipitation was highly episodic with little seasonality while evaporation occurred mostly during winter, resulting in a net evaporation of -15 cm and net freshwater flux of $+48 \text{ cm}$ over the deployment. INDEX

TERMS: 4504 Oceanography: Physical: Air/sea interactions (0312); 4247 Oceanography: General: Marine meteorology; 4219 Oceanography: General: Continental shelf processes; 4227 Oceanography: General: Diurnal, seasonal, and annual cycles; KEYWORDS: wind stress, heat flux, surface forcing, Georges Bank, Gulf of Maine

Citation: Beardsley, R. C., S. J. Lentz, R. A. Weller, R. Limeburner, J. D. Irish, and J. B. Edson, Surface forcing on the southern flank of Georges Bank, February–August 1995, *J. Geophys. Res.*, 108(C11), 8007, doi:10.1029/2002JC001359, 2003.

1. Introduction

[2] The U.S. Global Ocean Ecosystem (GLOBEC) Northwest Atlantic/Georges Bank program was designed to investigate the development of zooplankton and larval fish communities on Georges Bank, with special emphasis on the physical and biological processes which influence the population dynamics of four target species: the groundfish cod (*Gadus morhua*) and haddock (*Melanogrammus aeglefinus*), and their zooplankton prey (*Calanus finmarchicus* and *Pseudocalanus*). These species were chosen because they are important members of the Georges Bank and other North Atlantic ecosystems, and their populations are (likely) sensitive to changing climatic conditions, a growing concern for resource management. Georges Bank was chosen as the primary study site because the shallow bank with its clockwise around-bank circulation was thought to form a semi-closed or isolated environment for cod and haddock

that would be strongly affected by climate variability over the northeast margin of North America.

[3] In 1995, GLOBEC conducted the Georges Bank Stratification Study (GBSS) to investigate the physical processes which control the seasonal development of stratification along the southern flank of Georges Bank during spring and summer, and their influence on the distribution, abundance, health, and behavior of the target species during their early pelagic stages. A moored array was deployed from January to August to determine the surface wind stress and heat and moisture fluxes and to observe the onset and evolution of seasonal stratification over the southern flank with sufficient vertical and horizontal resolution that key physical processes could be identified and quantified. Moored measurements were also made to monitor stratification on the crest and the northeast peak.

[4] This paper describes the meteorological measurements made on Georges Bank during the 1995 Stratification Study which provide the first in situ data set comprehensive enough to allow direct estimation of the surface heat, moisture, and momentum fluxes there. As such it is an

important step toward quantifying the roles of different physical processes during the evolution and onset of the stratification. The site and seasonal cycles are summarized first, followed by descriptions of the moored instrumentation, the surface meteorological conditions, and the surface fluxes. Four representative meteorological events are described in greater depth, including a winter gale and a summer hurricane. Spatial variability is examined on Georges Bank by comparing these measurements on the southern flank with those at other sites.

[5] The ocean responses to these surface fluxes are described in the companion papers by *Lentz et al.* [2003] on the observed variability in water column heat and salt content on the southern flank and crest, *Brink et al.* [2003] on the near-surface Lagrangian flow and its wind-driven component, *Werner et al.* [2003b] on bottom bed form variability and sediment suspension, and *Werner et al.* [2003a] on the bottom tidal boundary layer. The role of realistic diurnal heating on summer stratification and residual circulation on the southern flank is investigated in the numerical model study by *Chen et al.* [2003].

2. Seasonal Surface Forcing

[6] Georges Bank is a shallow submarine bank located between the deeper Gulf of Maine and the continental slope (Figure 1). While the southern flank of Georges Bank extends directly into the Mid-Atlantic Bight to the west, Georges Bank is separated from Browns Bank and the Scotian Shelf by the relatively deep Northeast Channel (sill depth ~ 230 m). Semidiurnal tidal currents can reach speeds of 1 m/s over the shallow crest of Georges Bank, creating a region of vertically well-mixed water surrounded by a tidal mixing front (TMF) located near the 60-m isobath. Relatively fresh shelf water found on the bank is separated from more saline slope water by the shelf-slope front (SSF) located near the shelf break. The large seasonal variation of surface temperature over Georges Bank and the Gulf of Maine has long been attributed to a strong seasonal cycle in surface forcing [*Bigelow*, 1927; *Hopkins and Raman*, 1987; *Butman and Beardsley*, 1987; *Mountain et al.*, 1996].

[7] Wind stress on Georges Bank exhibits a clear seasonal cycle (Figure 2) [*Manning and Strout*, 2001]. The 1984–1999 monthly mean wind stress at NDBC buoy 44011 located on the southeastern flank of Georges Bank (Figure 1) has a clear maximum in winter and minimum in summer, veering from southeastward in winter to northeastward in June and July. Strong cyclogenesis frequently occurs over the central United States during the colder months, resulting in developing lows that tend to track toward the northeast on both sides of Georges Bank, leading to large wind stress fluctuations in all directions on the bank [*Miller*, 1946; *Mather et al.*, 1964; *Hopkins and Raman*, 1987]. The resulting synoptic scale (2–10 day) weather systems dominate wind stress variability over the bank from fall through early spring, with maximum variance in winter of ~ 0.2 N/m² in December through February. (An analysis of cyclone frequency for 1885–1980 shows more storms hit Georges Bank, the Gulf of Maine and Scotian Shelf than any other part of the eastern North American continental shelf [*Hayden and Smith*, 1982]. On average, 14 cyclones pass over the bank during winter (October–March) and

8 during summer (April–September). The standard deviation in cyclone frequency, an indication of interannual variability, is about 4 in both winter and summer.) Summer is marked by the passage of fewer and weaker weather systems, with the one notable exception being a tropical storm or hurricane once every six years on average [*Cry*, 1965].

[8] Surface heat flux on Georges Bank also exhibits a clear seasonal cycle. Estimates of monthly-mean net surface heat flux (Q_{NET}) and its four components, the shortwave (Q_{SW}) and long-wave (Q_{LW}) radiative fluxes and the sensible (Q_{SEN}) and latent (Q_{LAT}) air-sea fluxes, for the one degree square (40° – 41° N, 67° – 68° W) centered on the southern flank are shown in Figure 2. These estimates result from the Southampton Oceanography Centre (SOC) re-analysis of the 1980–1993 Comprehensive Ocean Atmosphere Dataset 1a by *Josey et al.* [1998]. During the colder months, the increase in Q_{LAT} and Q_{SEN} heat loss combined with decreased insolation produce a net surface cooling (negative Q_{NET}) from October through March, with a maximum cooling rate of 215 W/m² in December. Net surface heating occurs from April through September, with a maximum in June and July due to the seasonal maximum in insolation and minima in Q_{SEN} and Q_{LAT} associated with weak summer winds and warmer, more humid air. The annual mean heat flux has shortwave heating (~ 150 W/m²) opposed by latent heat loss (approximately -85 W/m²), long-wave loss (approximately -60 W/m²), and sensible heat loss (approximately -25 W/m²), resulting in a small net loss of approximately -20 W/m².

[9] The large seasonal cycle in Q_{NET} (380 W/m²) is caused by large changes in insolation and the air-sea fluxes. From June to December, shortwave heating decreases by about 200 W/m² while latent and sensible cooling increase by roughly 100 and 55 W/m², respectively. There is always net long-wave cooling, but the increase from June to December is only about 20 W/m². The SOC heat flux estimates for the rest of Georges Bank and adjacent waters exhibit similar seasonal cycles. There is little spatial variation in Q_{SW} and Q_{LW} , but latent and sensible heat loss increase toward the south, associated with the increase in sea surface temperature (SST) over the slope water and especially the Gulf Stream, where the largest net heat loss in the North Atlantic occurs in winter [*Bunker*, 1976]. The uncertainties in the SOC heat flux estimates are difficult to determine. The values for Georges Bank must be viewed with caution, since COADS wind stress estimates are roughly a factor of 2 larger than our estimates based on the in situ buoy data (Figure 2). This suggests that the air-sea flux components may be overestimated, which would result in a reduction of cooling caused by Q_{SEN} and Q_{LAT} . One objective of the Georges Bank Stratification Study was to estimate more directly the surface heat flux using a full suite of moored in situ meteorological measurements.

3. ST1 Moored Measurements

3.1. Instrumentation

[10] Meteorological measurements were made at the primary GBSS site ST1 from 1 February to 23 August 1995. This site was located on the 76-m isobath, roughly halfway between the tidal mixing front and the shelf-slope front (Figure 1). The ST1 surface discus buoy supported

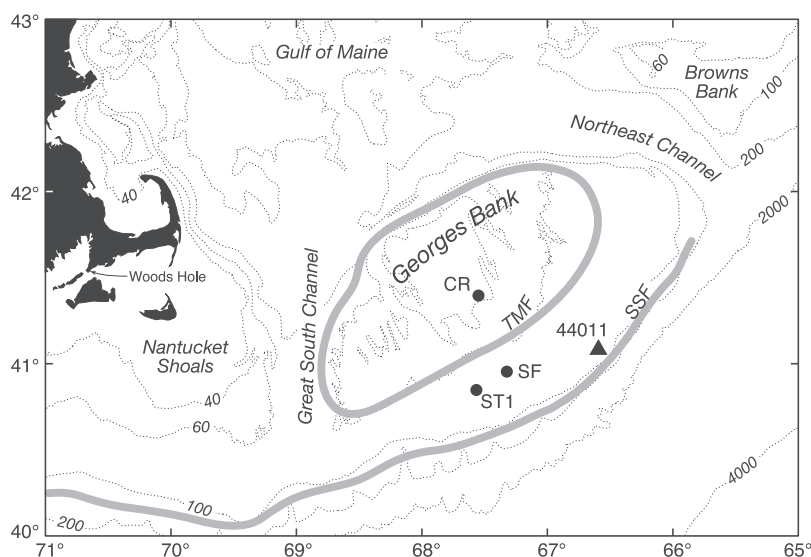


Figure 1. Map showing topography of Georges Bank and adjacent Gulf of Maine and approximate locations of the tidal mixing front (TMF) and the shelf-slope front (SSF). This study analyzes surface measurements made during January–August 1995 at the Stratification Study site 1 (ST1), the long-term southern flank (SF) and crest (CR) sites, and at NDBC buoy 44011. The water depth at these sites is 76, 75, 43, and 88 m, respectively. The 40-, 60-, 100-, 200-, 2000-, and 4000-m-depth contours are shown.

two independent meteorological packages, a Vector-Averaging Wind Recorder (VAWR) [Dean and Beardsley, 1988] and an Improved Meteorological Instrumentation (IMET) package [Weller et al., 1990; Hosom et al., 1995] (Figure 3).

Each system measured wind speed (WS) and direction (WD), air (T_A) and sea surface (T_S) temperatures, relative humidity (RH) and incident short (SW) and long-wave (LW) radiation, while the IMET also recorded precipitation

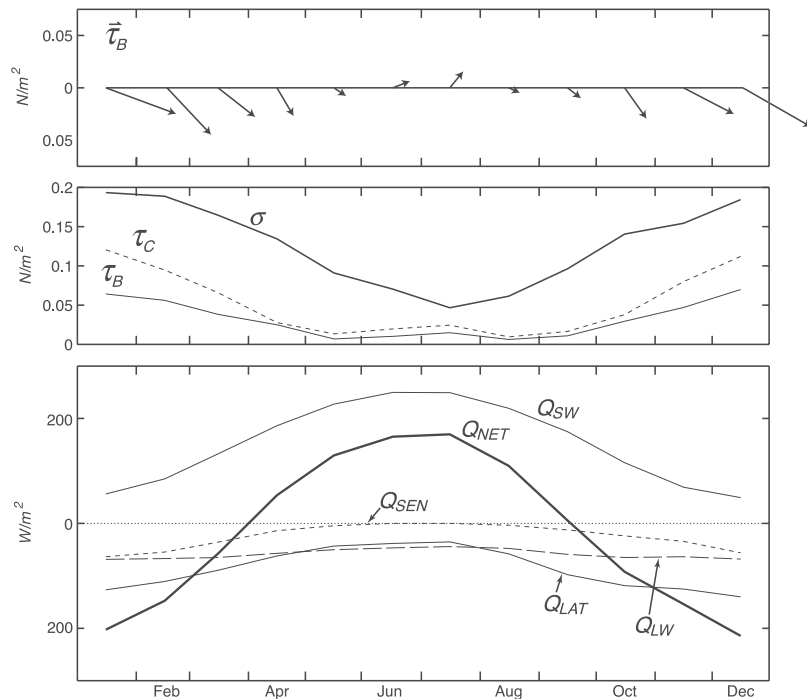


Figure 2. Seasonal cycles of surface forcing on Georges Bank: (top) wind stress (τ_B) at NDBC buoy 44011; (middle) wind stress amplitude (τ_B) and deviation (σ) at buoy 44011, plus the SOC wind stress amplitude (τ_C); and (bottom) the SOC surface heat flux components for the one degree square (40°N – 41°N , 67°W – 68°W) centered on the southern flank. The net heat flux Q_{NET} is the sum of the shortwave (Q_{SW}), long-wave (Q_{LW}), sensible (Q_{SEN}) and latent (Q_{LAT}) components; positive values indicate a heat flux into the ocean. Wind stress is computed using the Large and Pond [1981] neutral drag formulation and monthly averages computed for 1984–1999. The monthly SOC values were averaged over 1980–1993.

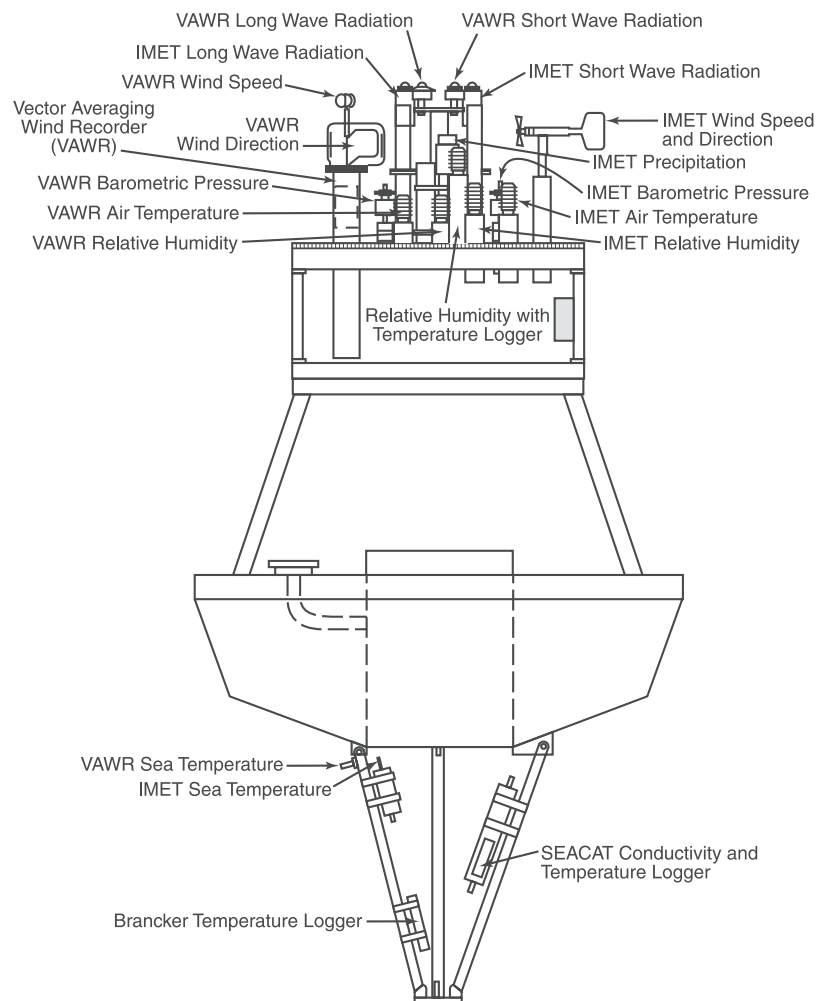


Figure 3. Schematic of ST1 surface discus buoy, showing the meteorological and oceanographic instruments deployed on this mooring. A steering vane (not shown) attached to one of the tower legs oriented the buoy into the wind so that the wind, air temperature, and relative humidity sensors were upstream, facing into the wind.

(P) and air pressure (BP). A steering vane was used to orient the discus buoy so that the wind, air temperature/relative humidity, and air pressure sensors were heading into the wind with minimal flow distortion. The radiation sensors were placed high on the buoy to minimize shadowing. The sea surface temperature sensors were mounted on the buoy bridle, together with a SeaCat temperature and conductivity recorder. Just below the bridle was attached a Vector-Measuring Current Meter (VMCM) to measure the near-surface horizontal current at 5.2-m depth.

[11] Despite a series of storms with winds in excess of 18 m/s and short, steep waves that battered the buoy, the buoy remained on station and most VAWR and IMET sensors returned complete records. Daily monitoring via ARGOS indicated that one long-wave sensor failed on 1 March and the IMET and VAWR wind sensors failed on 16 May and 3 June, respectively. The long-wave sensor was replaced on 11 June, and both IMET and VAWR wind sensors were replaced on 11 July. NDBC buoy 41011 wind data were used to estimate the missing ST1 wind data with an RMS uncertainty of ± 1.5 m/s. Data collected with other

VAWR and IMET sensors were compared to produce the final meteorological data set for scientific analysis.

[12] The different sensor systems used to produce this final data set are listed in Table 1, together with estimates of in situ measurement uncertainties. Many factors contribute to measurement uncertainty, including calibration error, sensor degradation and drift, sensor placement, flow distortion and turbulence, mooring motion, and shielding problems. For example, the air temperature sensor was placed in a Gill radiation shield to reduce overreading due to solar heating, which can be of order several $^{\circ}\text{C}$ during sunny calm conditions [Payne, 1987]. For wind speeds above 5 m/s, this error is reduced to $\pm 0.3^{\circ}\text{C}$ on sunny days. The long-wave sensor was also sensitive to solar heating; however, this effect was removed in postprocessing by regression using the measured insolation.

[13] The cup anemometer and rain gauge are both affected by flow distortion and turbulence. The wind speed uncertainty in Table 1 is for steady flow conditions; the issue of unsteady flow and cup over speeding is discussed in the next section. The precipitation record is corrected in

Table 1. Specifications of the Moored Instrumentation Used to Collect Air-Sea Data Presented in This Study^a

Site	Variable	Sensor Type and Model	Sensor Height, m	In Situ System Accuracy	Sample Method	Record Interval, min	Reference
ST1	wind speed	three-cup anemometer, R.M. Young	3.3	$\pm 2\%$ ⁽¹⁾	15-min vector average	15	1, 2
	wind direction	integral vane/vane follower/compass, EG&G/WHOI	3.1	$\pm 5.6^\circ$	15-min vector average	15	1
	air temperature	thermistor, Roton Model MP-101A, Gill Radiation Shield	2.7	$\pm 0.3^\circ\text{C}$ for winds > 5 m/s ⁽²⁾	1-min average	1	1, 3, 5
	relative humidity	Hair, Roton Model MP-101A	2.7	$\pm 4\%$	3.5-s average	1	1, 3, 5
	barometric pressure	Digiquartz, Paroscientific Model 215-AW, Gill Pressure Port	2.8	± 0.6 mbar for winds < 20 m/s ⁽³⁾	2.6-s average	15	1, 3
	shortwave radiation (insolation)	pyranometer, Eppley Model 8-48	3.4	$\pm 4\%$ ⁽⁴⁾	15-min average	15	1, 2, 4
	long-wave radiation	pyrgeometer, Eppley Model PIR	3.4	± 10 W/m ² ⁽⁵⁾	15-min average	15	1
	precipitation	self-siphoning rain gauge, R.M. Young Model 50203	3.1	± 1.3 mm/hr during rainfall, otherwise ± 0.3 mm/hr ⁽⁶⁾	1-min average	1	1, 6, 7, 8
	water temperature	thermistor, WHOI	-1.0	$\pm 0.1^\circ\text{C}$ ⁽⁷⁾	1-min average	1	1, 3
	current speed	dual propellers, VMCM	-5.2	$\pm 1\%$	7.5-min vector average	7.5	1, 9
current direction	fluxgate compass, VMCM	-5.2	$\pm 5^\circ$	7.5-min vector average	7.5	1, 9	
CR and SF	air temperature	thermistor, thermometrics, Gill Radiation Shield	2.8	$\pm 0.3^\circ\text{C}$ for winds > 5 m/s ⁽²⁾	hourly average of 60 1-min samples	60	1
	water temperature	thermistor, Sea-Bird Model SBE-3	-1.0	$\pm 0.1^\circ\text{C}$ ⁽⁷⁾	hourly average of 60 1-min samples	60	1
44011	wind speed	vane-directed propeller	5.0	± 1 m/s	8-min vector average	60	10
	wind direction	vane/compass	5.0	$\pm 10^\circ$	8-min vector average	60	10
	air temperature	thermistor	4.0	$\pm 1^\circ\text{C}$	8-min average	60	10
	barometric pressure	variable capacitance	0.0	± 1 mbar	8-min average	60	10
	water temperature	thermistor	-1.0	$\pm 1^\circ\text{C}$	8-min average	60	10
	significant wave height	accelerometer	in-hull	± 0.2 m	20-min average	60	10
	dominant wave period	accelerometer	in-hull	± 1 s	20-min average	60	10

^aNotes (1) does not include effects of cup overspeeding or flow distortion (see section 4); (2) includes effects of solar heating of sensor housing at low wind speeds; (3) includes effects of pressure port in higher winds; (4) includes estimated effects of sensor tilt as pyranometer was not gimballed; (5) includes correction for internal heating due to daily solar heating; (6) does not include correction for wind on collection efficiency; and (7) includes estimated effects of sensor location below sea surface. References are as follows: 1, *Alessi et al.* [2001]; 2, *Beardsley et al.* [1998]; 3, *Weller et al.* [1990]; 4, *MacWhorter and Weller* [1991]; 5, *Payne* [1987]; 6, *Yang et al.* [1998]; 7, *Yuter and Parker* [2001]; 8, *Serra et al.* [2001]; 9, *Beardsley* [1987]; and 10, *Hamilton* [1980].

postprocessing for wind effects on the collection efficiency of the rain gauge using equation (7) from *Yang et al.* [1998]. Owing to the water flow around the buoy, the water temperature record is thought to represent the temperature at an effective depth of 0.5 m (R. Trask, personal communication, 1995). The uncertainty in Table 1 is an estimate of the difference in temperature between 0.5 m and the surface under all but very calm conditions. While little is known about current shears between the surface and 5 m at ST1, their influence on the computed wind stress should be marginal, especially during the stronger wind events, when the surface mixed layer extends well below the 5-m VMCM. How these uncertainties combine to produce uncertainties in the surface fluxes is discussed in section 4.

[14] Air and sea-surface temperature were also measured during this period at the GBSS crest site CR (water depth 43 m) and the long-term southern flank site SF (Figure 1). CR was located 60 km north of ST1, within the region of strong tidal mixing. SF was located 24 km northeast of ST1

along the 76-m isobath. NDBC buoy 44011 recorded wind speed and direction, air and water temperature, and barometric pressure. The buoy also measured surface wave-height variability with an accelerometer, and recorded significant wave height and mean and significant wave period. Table 1 also lists the CR, SF, and buoy 44011 instrumentation and in situ measurement uncertainties (see *Alessi et al.* [2001] for additional details about the GBSS instrumentation, sensor comparisons, system uncertainties, and methods used to produce the final data set considered here).

3.2. Meteorological Measurements

[15] Time series of the ST1 meteorological measurements are shown in Figure 4. Atmospheric lows past ST1 frequently, causing a succession of strong wind events during the deployment period. Wind speeds exceeded gale-force (> 14.7 m/s) once each during early February and early April, and twice in early May. A transition between this initial period of frequent lows and strong winds (“winter”)

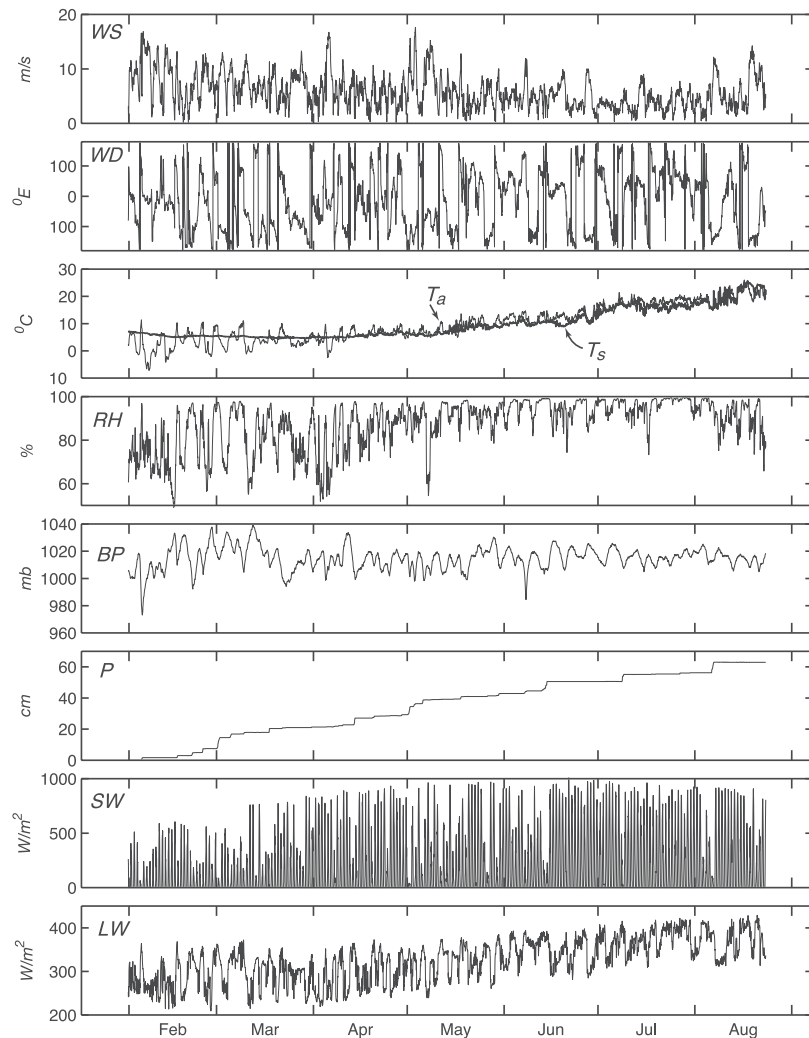


Figure 4. Time series of hourly ST1 meteorological measurements, starting at the top with wind speed, wind direction counterclockwise relative to east, air and sea surface temperatures, relative humidity, barometric pressure, accumulated precipitation, and downward short and long-wave radiation. Winter and summer analysis periods are shown at top.

to less frequent lows and weaker winds (“summer”) occurs during mid-May. During this “winter” period, the winds are nearly circularly polarized, with the principal axis oriented toward the ESE (Table 2). In “summer,” the winds are weaker (the kinetic energy is about one-half) and more polarized in the along-bank direction with the principal axis pointing toward the northeast. In both seasons, the wind variance is concentrated in the 2–10-day synoptic weather band (Figure 5), with more cyclonic (60%) than anticyclonic (40%) variability. The dominant event period (computed as 2π divided by the kinetic energy averaged frequency), which characterizes the mean time between events, increases from roughly 5 days in winter to 6.5 days in summer.

[16] The other variables also exhibit a seasonal change from winter to summer. T_S warms from a minimum of 4.4°C in March to a maximum of 25.5°C in August, while T_A climbs from a winter minimum of -7.2°C in February to a maximum of 26°C in August. The air is on average cooler than the ocean in winter, but with large differences as winter lows carry cold, relatively dry continental air

across Georges Bank. In summer, the air is warmer than the ocean but tends to track SST closer as warmer, more humid, marine air is carried toward the northeast along the shelf. BP shows no change on average but reduced variability in summer, consistent with the weaker, less-frequent weather systems during summer. Both downward SW and LW radiation increase from winter into summer, the latter due in part to the increased air temperature and humidity during summer. The net accumulation of precipitation decreased from about 39 cm in winter to 28 cm in summer. Much of this difference was due to a series of storms near 1 March.

4. ST1 Surface Fluxes

[17] We consider here the surface momentum, heat, and net-moisture fluxes at ST1 computed using bulk methods as described by *Beardsley et al.* [1998]. The surface momentum flux (wind stress) was computed using the Tropical Ocean Global Atmosphere/Coupled Ocean Atmosphere Response Experiment (TOGA/COARE) version 2.5

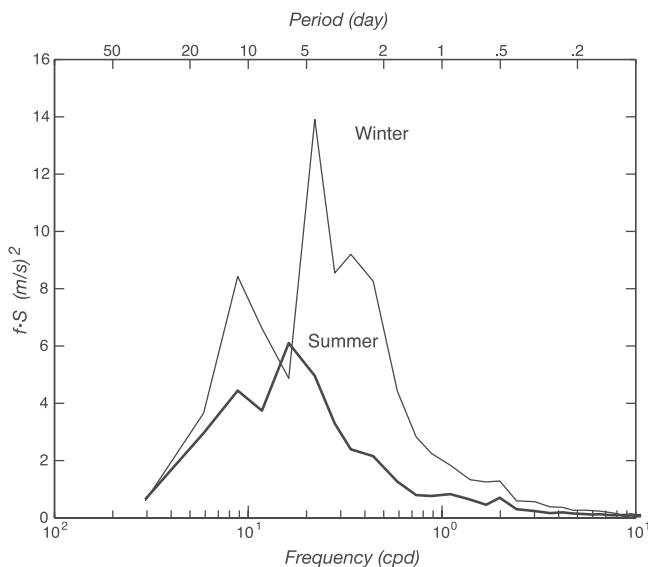


Figure 5. ST1 wind kinetic energy spectra for winter and summer periods. Frequency times spectral density is plotted versus log frequency (area-preserving) so that frequency bands with equal areas under the curve contain equal kinetic energy.

(TC2.5) formulation [Fairall *et al.*, 1996]. The net surface heat flux Q_{NET} into the ocean is the sum of four components: Q_{SW} and Q_{LW} are the net downward short- and long-wave radiation fluxes, Q_{SEN} the sensible heat flux due to air-sea temperature differences, and Q_{LAT} the latent heat flux due to water-vapor transport. Q_{SW} is simply the measured insolation SW corrected for reflection using Payne's [1972] ocean albedo factor. Q_{LW} is the measured downward long-wave flux LW minus the upward grey body radiation from the ocean surface computed using the measured surface temperature T_S . Q_{SEN} and Q_{LAT} are proportional to the air-sea temperature and specific humidity differences, respectively, multiplied by the magnitude of the wind velocity minus the surface current velocity. These air-sea fluxes were computed using the TC2.5 formulation without correction for skin temperature effects, which are negligible under typical conditions on Georges Bank. The net moisture flux into the ocean is the difference between the measured (downward) precipitation P and the (upward) moisture flux associated with evaporation E . Here negative E indicates a decrease in sea-surface height due to positive evaporation, so that the net (downward) freshwater flux is $P + E$ (see Pawlowicz *et al.* [2001] for a full description of the bulk methods used here).

[18] Uncertainties in these surface fluxes are estimated here using the following approach. Hourly time series of these fluxes computed with the basic variables (the base case) are compared with those computed using input variables biased upward and downward by the measurement uncertainties in Table 1. The means and standard deviations of the difference time series are listed in Table 3 for the individual measurement uncertainties. These are combined to give the largest positive and negative biases listed in the last column in Table 3.

[19] Uncertainty in wind stress is due almost entirely to two factors, uncertainty in the measured wind and use of the

TC2.5 drag formulation developed for equilibrium deep-ocean sea-state conditions. The VAWR and IMET hourly vector wind speeds showed an -11% difference when both sensors were working, suggesting that the VAWR cup anemometer experienced overspeeding in unsteady conditions (in comparison to the IMET prop and vane sensor). Since earlier comparisons [e.g., Friehe *et al.*, 1984; Beardsley *et al.*, 1997] suggested smaller values or no VAWR cup overspeeding, a value of -6% was used here to estimate the sensitivity of the ST1 surface fluxes to possible cup overspeeding in Table 3. Shipboard observation of the ST1 discus buoy and surface wave height and period measurements made at buoy 44011 both show the ST1 buoy experienced large steep waves during the stronger winter storms. Calculations of wind stress made with several new sea-state-dependent drag formulations (Appendix A) suggest that the wind stress was enhanced during several winter storms, but that over most of the deployment, the enhancement was not significant (less than 2% on average for stresses above 0.1 N/m^2). For this reason, we chose to present here wind stress as computed using the TC2.5 equilibrium drag formulation. The sea-state-enhanced wind stress will be discussed later in section 5.1 where the surface forcing during one February storm with large surface waves is described in detail and the estimated maximum wind stresses were increased by 5–10%.

[20] Uncertainties in all the in situ surface measurements contribute to uncertainty in the net surface heat flux. Owing to the relative importance of insolation and long-wave cooling over the winter through summer deployment, uncertainties in the incident radiation measurements contribute comparable uncertainties as do the air-sea flux components. Uncertainties in air temperature and relative humidity contribute most to the sensible and latent heat flux (and accumulated evaporation) uncertainties, with sea-surface temperature and wind speed uncertainties contributing less.

4.1. Wind Stress

[21] The surface wind stress is shown in Figure 6 and simple statistics based on hourly data given in Table 4. As suggested by the measured winds, larger and more-frequent wind stress fluctuations occur in the winter period, with an

Table 2. Basic Statistics of the ST1 Surface Measurements for the “Winter” Period (1800 UT 31 January to 1800 UT 13 May 1995) and “Summer” Period (1800 UT 13 May to 1600 UT 23 August)^a

Variable	Winter	Summer	Units
Wind			
Major axis	5.5	4.5	m/s
Minor axis	5.1	2.6	m/s
Theta	-14	42	°E
KE	22.7	11.4	(m/s) ²
T	5.1	6.5	day
Speed	7.1 (3.4)	4.7 (2.5)	m/s
T_A	4.6 (3.2)	15.2 (4.3)	°C
T_S	5.5 (0.6)	14.1 (4.7)	°C
$T_A - T_S$	-1.0 (3.1)	1.1 (1.7)	°C
RH	81 (12)	94 (5)	%
BP	1014 (10)	1015 (6)	mbar
SW	143 (226)	247 (306)	W/m ²
LW	294 (40)	357 (35)	W/m ²
ΔP	39	28	cm

^aStandard deviations are shown in parenthesis.

Table 3. Sensitivity of Wind Stress, Heat Flux, and Accumulated Evaporation to Uncertainties in the Basic Near-Surface Meteorological and Ocean Measurements Made at ST1 During the 1 February to 23 August 1995 Deployment^a

Variable	Units		$T_A \pm 0.3^\circ\text{C}$	$T_S \pm 0.1^\circ\text{C}$	RH $\pm 4\%$	SW $\pm 4\%$	LW $\pm 10 \text{ W/m}^2$	U -6%	Maximum Combined Uncertainty
τ	dyne/cm ²	mean	± 0.01	$< \pm 0$	$< \pm 0$	–	–	–0.13	$\pm 8\%$
		std.	0	0	0	–	–	± 0.17	± 0.17
Q_{NET}	W/m ²	mean	± 6	± 3	± 7	± 8	± 10	1	± 35
		std.	± 3	± 1	± 5	± 11	–	± 5	± 13
Q_{SW}	W/m ²	mean	–	–	–	± 8	–	–	± 8
		std.	–	–	–	± 1	–	–	± 11
Q_{LW}	W/m ²	mean	–	± 1	–	–	± 10	–	± 11
		std.	–	0	–	–	–	–	0
Q_{SEN}	W/m ²	mean	± 3	± 1	$< \pm 0$	–	–	0	± 4
		std.	± 2	± 1	0	–	–	± 2	± 3
Q_{LAT}	W/m ²	mean	± 3	± 1	± 7	–	–	1	± 12
		std.	± 2	± 1	± 5	–	–	± 3	± 6
E	cm	mean	± 1.0	± 0.4	± 2.2	–	–	0.5	± 3.8
		std.	± 0.6	± 0.2	± 1.2	–	–	± 0.2	± 1.2

^aThe mean and standard deviation are computed between hourly values calculated with the ST1 basic data and those biased by the uncertainty in each variable. The last column lists the combination of uncertainties that give the maximum (positive/negative) biases. Units of wind stress, heat flux, and accumulated evaporation are dynes/cm² ($=0.1 \text{ N/m}^2$), W/m² and cm, respectively. A 6% reduction in wind speed leads to a 14% reduction in wind stress, which we split in half for a crude estimate of combined uncertainty. The heat flux values are rounded to the nearest integer. Values of the mean and standard deviation less than the least significant figure given for each variable are listed as 0. A positive value of E means a reduction in the depth of water evaporated (e.g., $E = 1$ means 1 less cm of water lost to the atmosphere during the deployment).

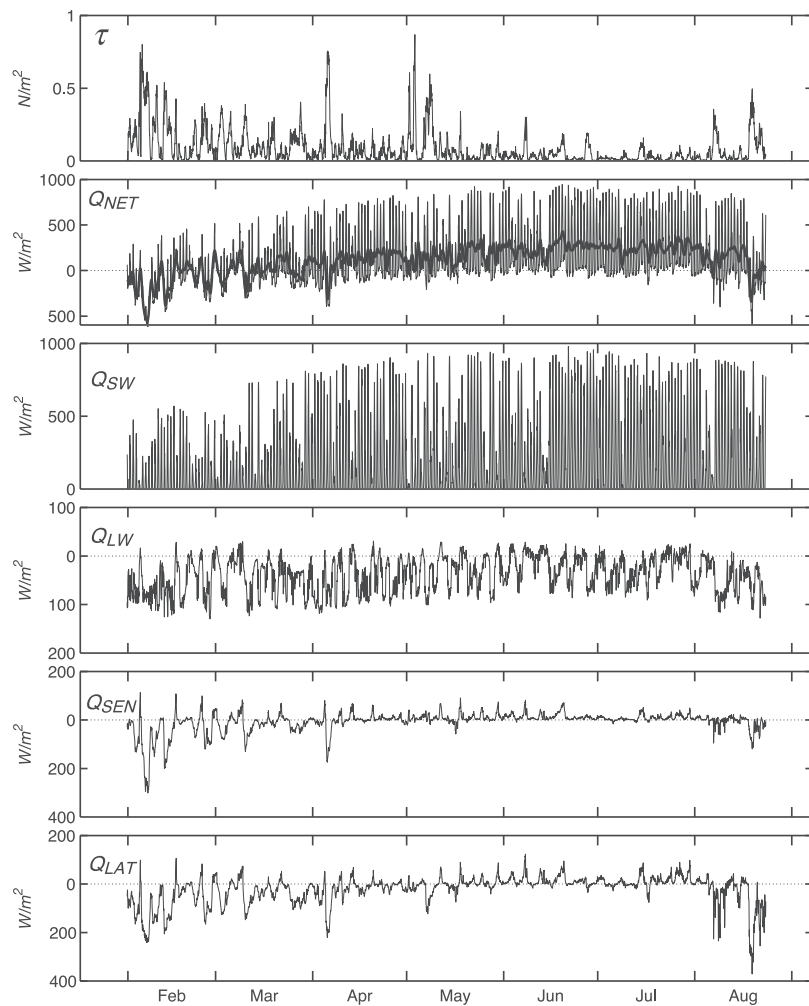


Figure 6. Time series of hourly ST1 surface wind stress and heat flux, starting at the top with wind stress magnitude, net heat flux, short- and long-wave radiative fluxes, and sensible and latent fluxes. Note changes in vertical scale for different heat flux components. The low-pass filtered net heat flux (thick curve) is shown to emphasize seasonal and synoptic-band variability.

Table 4. Basic Statistics of the ST1 Surface Fluxes for the “Winter” Period (1800 UT 31 January to 1800 UT 13 May 1995) and “Summer” Period (1008 UT 13 May to 1600 UT 23 August)^a

Variable	Winter	Summer	Units
Wind stress			
τ_X	0.033 (0.141)	-0.002 (0.058)	N/m ²
τ_Y	-0.052 (0.117)	-0.002 (0.058)	N/m ²
Major axis	0.143	0.073	N/m ²
Minor Axis	0.115	0.032	N/m ²
Theta	-16	43	°E
Amplitude	0.130 (0.144)	0.048 (0.064)	N/m ²
Q_{NET}	27 (246)	207 (296)	W/m ²
Q_{SW}	133 (215)	233 (294)	W/m ²
Q_{LW}	-47 (39)	-29 (32)	W/m ²
Q_{SEN}	-19 (54)	6 (20)	W/m ²
Q_{LAT}	-40 (58)	-3 (52)	W/m ²
E	-0.9	-1.2	mm/d
P	1.8	5.0	mm/d
$E + P$	0.9	3.8	mm/d

^aStandard deviations are shown in parenthesis. The average evaporation, precipitation, and $E + P$ rates are given in millimeters per day.

average magnitude of 0.13 N/m² and maximum stresses above 0.5 N/m² during four storms. The winter fluctuations tend to be omnidirectional, and larger by a factor of about 2 than the mean vector wind stress directed toward the east-southeast (Figure 7). In summer, the mean wind stress magnitude is about one third of that in winter, with maximum stresses occurring in August during passage of tropical storm Felix. Fluctuations are weaker in summer but more strongly polarized, with the major axis aligned toward the northeast (roughly parallel to the topography of the southern flank). As a result, fluctuations in the along-bank wind stress component in summer are roughly a factor of 2 smaller than in winter, while cross-bank fluctuations are a factor of 4 smaller in summer (Figure 7). The vector mean

stress during the summer is essentially zero. (These results remain roughly unchanged when Felix is excluded from the summer record.) Fluctuations in both seasons contain comparable contributions from the clockwise and counterclockwise turning components.

4.2. Heat Flux

[22] The net surface heat flux and its variability are dominated by the shortwave flux component (Figure 6). The deployment period starts about 48 days before spring equinox and extends 64 days past summer solstice, so that the large seasonal increase in insolation is captured. Spectra of Q_{NET} and Q_{SW} exhibit clear peaks at 1 and 2 cpd (Figure 8), consistent with the clipped shape of daily insolation. Clouds and marine fog cause variations in Q_{SW} on timescales from minutes to days, with some limited (visual) correlation between reduced Q_{SW} and increased wind stress in Figure 6. The correlation between daily Q_{SW} and wind stress averaged over daylight hours is weak ($r^2 = -0.30$) but significant at 95% confidence only during the winter analysis period. Storms can bring clear skies as well as clouds, and marine clouds can form during summer under conditions of very weak winds.

[23] The net long-wave flux exhibits weaker and less-frequent fluctuations in summer than winter, with most of its variability occurring in the 2–10 day weather band. The sensible and latent heat fluxes have similar seasonal behavior, with both being more negative (ocean cooling) with larger fluctuations in the 2–10 day weather band in winter. In summer, typical fluctuations in Q_{SEN} and Q_{LAT} are weaker due to reduced winds and tend to be positive (ocean warming) due to the air being warmer than the ocean surface. Tropical storm Felix caused relatively large sensible and latent heat loss in late August, which in combination with an increased long-wave cooling and reduced shortwave

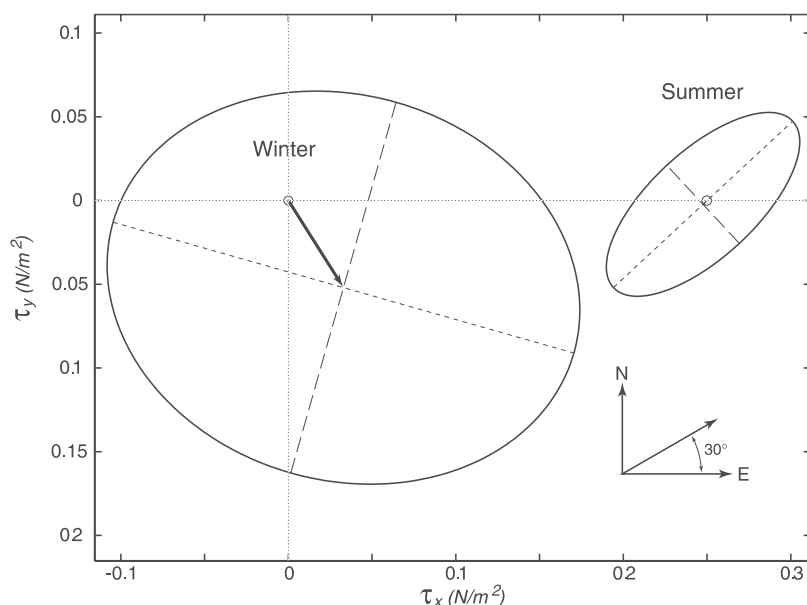


Figure 7. Mean and principal axes of ST1 wind stress during (left) winter and (right) summer periods. The principal axes are plotted at the tip of the mean wind stress vector (the summer mean wind stress vector is too small to show in this plot). The mean orientation of the topographic contours surrounding ST1 is 30° counterclockwise relative to east.

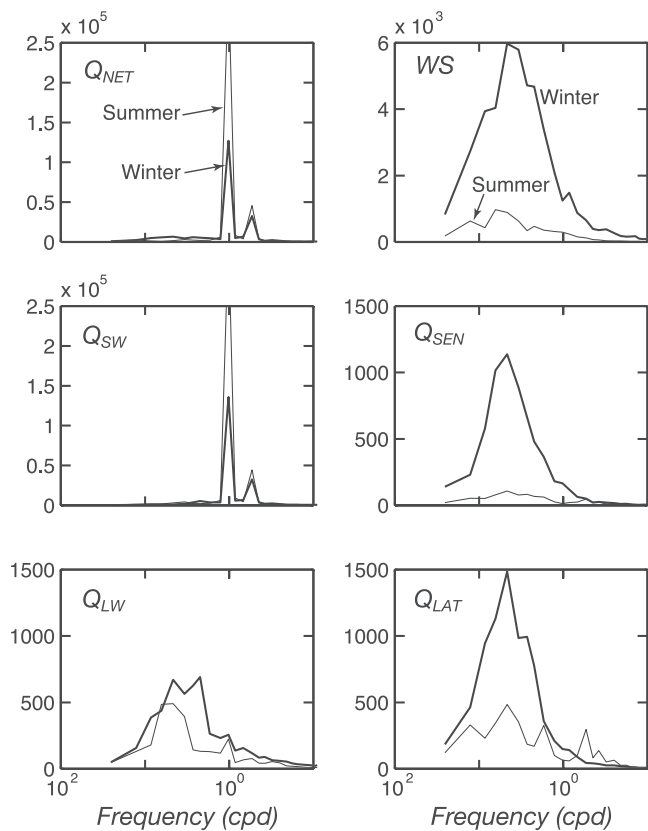


Figure 8. Spectra of ST1 surface heat flux and wind stress for winter and summer periods. Note changes in vertical scales. Units: wind stress (N/m^2); heat flux (W/m^2).

warming, produced net cooling during this period. On average, the winter period was characterized by weak net heating ($\sim 30 W/m^2$), with shortwave gain mostly offset by long-wave, sensible and latent heat loss (Table 4). In summer, increased shortwave gain and reduced long-wave loss and very weak air-sea fluxes combine to produce strong net surface warming ($\sim 210 W/m^2$). This large seasonal increase in net surface heating drives the formation of the seasonal thermocline (pycnocline) over Georges Bank [Lentz et al., 2003; Werner et al., 2003a].

4.3. Freshwater Flux

[24] The 1995 Stratification Study marked the first time (to our knowledge) that self-contained moored precipitation measurements were made in the Gulf of Maine. Once corrected for the effects of wind on the gauge’s precipitation capture efficiency following Yang et al. [1998] and Yuter and Parker [2001], the ST1 precipitation record allows examination of the net surface fresh water flux, the difference between precipitation and evaporation, where evaporation is estimated from the latent heat flux.

[25] Precipitation on Georges Bank was highly episodic throughout the 8-month deployment (Figure 9). Precipitation was generally associated with the passage of cold fronts over the bank, but not all cold fronts or low-pressure systems caused rain on Georges Bank. On the basis of hourly precipitation rates, light (<0.25 cm/hr), moderate, and heavy (>0.75 cm/hr) precipitation occurred roughly 4.9, 1.5, and 0.3% of the time during the deployment, respectively.

Precipitation events with heavy rains occurred only 7 times, but these events contributed a total of 36.5 cm freshwater, roughly 58% of the total precipitation recorded at ST1 (63.0 cm).

[26] Evaporation at ST1 occurred primarily during February through April, when winter low-pressure systems carried colder, drier continental air across the relatively warm waters on Georges Bank, resulting in strong winds and large specific-humidity differences causing significant evaporation (up to -0.03 cm/hr). Periods of weak surface condensation conditions began to occur in May, when warm moist marine air was carried over relatively cool bank waters, resulting in a weak latent heat flux into the ocean that we interpret here as surface condensation [Beardsley et al., 1998]. The passage of Felix in mid-August caused strong evaporation at ST1. This low was blocked to the west by an advancing cold front that moved eastward over Georges Bank. The resulting flow carried cooler drier continental air over ST1, with large latent heat loss and

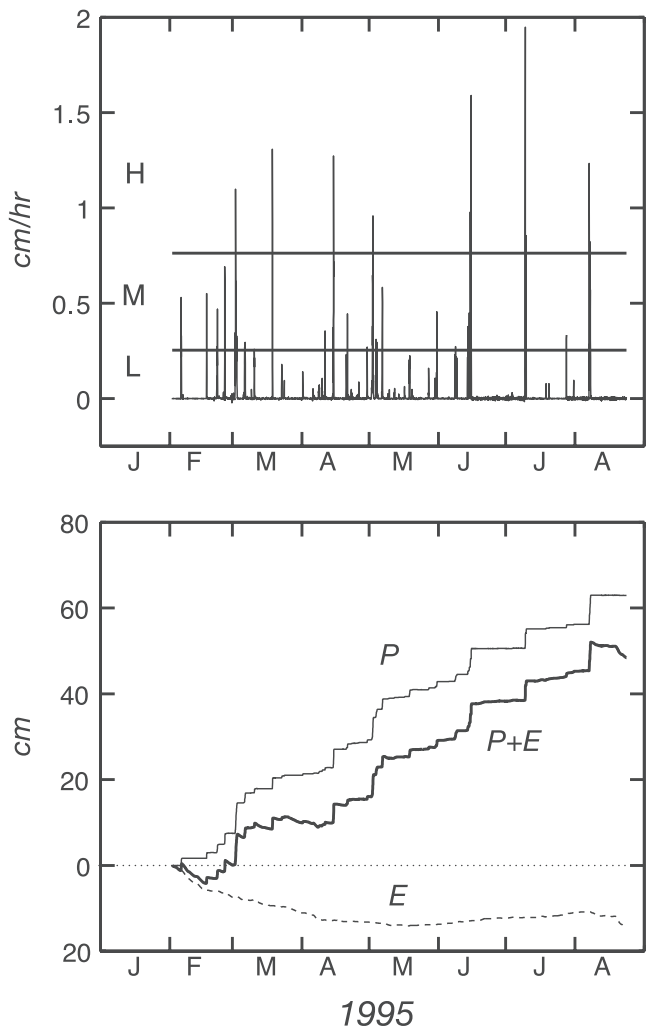


Figure 9. Precipitation and freshwater flux at ST1: (top) precipitation rate in cm/hr, with classification into light (L), moderate (M), and heavy (H) rainfall indicated; and (bottom) net accumulated precipitation P , evaporation E , and net freshwater flux $P + E$ into the ocean in centimeters.

evaporation (up to -0.05 cm/hr). The net freshwater flux $P + E$ at ST1 is generally positive, but with short periods of net loss associated with strong evaporation events and rapid increases due to precipitation events. Over the 8-month ST1 deployment, the net evaporation was -14.8 cm, giving a net freshwater flux $P + E = 48.2$ cm, a reduction of 24% of the total precipitation. This net ST1 $P + E$ flux plays a small but significant role in the salt balance on Georges Bank [Lentz *et al.*, 2003].

5. Surface Flux Events

[27] The passage of weather systems near Georges Bank cause the largest surface momentum and air-sea heat fluxes. In this section, we describe in more detail the surface fluxes at ST1 during four storms that are representative of different synoptic conditions characteristic of the Georges Bank and the outer New England continental shelf. These events include a winter “nor’easter,” a winter low moving up the St. Lawrence River valley, a pair of spring lows moving up along the coast, and the passage of a strong tropical depression south of the bank.

5.1. February Nor’easter

[28] On 2–3 February, a weak low moved northeastward from Maine into the Gulf of St. Lawrence, bringing a southward flow of cool ($\sim 0^\circ\text{C}$), relatively dry (RH ~ 70 – 80%) air across Georges Bank, with wind speeds at ST1 of 8–10 m/s (Figure 10). As this low moved further east on late 3 February and winds on Georges Bank weakened, a new low-pressure system developed over the Mississippi River valley and began to move eastward. On 4 February, this low moved to the Chesapeake Bay, then rapidly northeastward along the coast, reaching the Bay of Fundy on 5 February and the Gulf of St. Lawrence on 6 February. As the low reached the coast on 4 February, it intensified, with its center pressure dropping from 1002 mbar (0000 UT 4 February) to 973 mbar (0000 UT 5 February) to 962 mbar (1200 UT 5 February), a total drop of 40 mbar in 36 hours, with a peak drop of 30 mbar in 24 hours! This rapidly developing storm is a good example of the explosive Type II cyclogenesis that occurs along the U.S. east coast during winter [Bluestein, 1993].

[29] The center of this storm passed close to the north side of Georges Bank at about 0600 UT 5 February, causing the rapid drop in pressure at ST1 and clockwise rotation of the wind from northwestward to eastward (Figure 11). As the storm approached Georges Bank on 4 February, it brought relatively warm, moist marine air with increased cloudiness. Peak wind speeds just before and after the low-passed Georges Bank were 16–17 m/s, then dropping to 13–15 m/s during 6–7 February as this low merged with a second low over Newfoundland. As the storm was passing Georges Bank, the associated cold front passed ST1, causing moderate rain (average precipitation 0.28 cm/hr) during the first 5 hours on 5 February, followed by falling air temperature and relative humidity (reaching lows of about -7°C and 77% on 7 February).

[30] This winter cyclone produced strong surface fluxes at ST1 (Figure 11). The wind stress exceeded 0.7 N/m² just before and after the storm center passed north of Georges Bank, then was a relatively steady 0.5 N/m² directed east to

east-southeastward during 6–7 February before decreasing to less than 0.1 N/m² by early 8 February. As the storm approached Georges Bank, the net heat flux into the ocean became weakly positive due to the warm, moist air and strong winds driving both sensible and latent heat into the ocean and the heavy low-cloud cover reducing both the shortwave heating and net long-wave cooling to roughly zero. After the storm center passed the bank and the winds became more steady and eastward and air temperatures and RH fell toward their minima, the sensible and latent heat loss became substantial, reaching maximum 12-hour-averaged values of $Q_{SEN} = -273$ W/m² and $Q_{LAT} = -230$ W/m² during 0000–1200 UT 7 February, contributing 47% and 39% of the net flux $Q_{NET} = -583$ W/m². During this same 12-hour period, the entire sensible flux and roughly 70% of the latent flux were related to the large air-sea temperature difference ($T_A - T_S = -12.1^\circ\text{C}$), with only 30% of the latent flux due to the reduced relative humidity; in comparison, the net radiative component was small ($Q_{SW} + Q_{LW} = -80$ W/m²), contributing only 14% of the net heat flux. During this storm, the sensible and latent fluxes were approximately linearly correlated ($r^2 = 0.91$). A linear fit for the period 3–8 February gives $Q_{LAT} = (-40 \pm 13$ W/m²) + $(0.76 \pm 0.05) \times Q_{SEN}$, giving an effective Bowen ratio $B = Q_{LAT}/Q_{SEN} \approx 0.76$ (Figure 12).

[31] This winter “bomb” produced the largest Q_{SEN} loss and second largest Q_{LAT} loss during the entire ST1 deployment, which when combined with the seasonally low insolation and reduced long-wave radiative loss due to cold surface temperatures, resulted in the largest net heat loss during the 8-month measurement period. This storm also produced the largest waves measured on Georges Bank during the deployment (Figure 11). At buoy 44011 on eastern Georges Bank, the approaching storm built the seas up from a significant wave height H_S of about 2 m to 8 m during the last 9 hours of 4 February. The dominant wave period also jumped to about 9 s during this period, corresponding to a wavelength of 140 m and wave steepness of 0.2, indicative of nonlinear wave dynamics [Kraus and Businger, 1994]. As the storm passed the bank, wave height remained initially high, then decreased to about 5 m on 7 February before dropping to below 2 m on late 8 February. This rapid change in sea state as the storm approaches and passes the bank is thought to result in higher wind stress. Calculations with three new sea-state-dependent drag parameterizations (Appendix A) suggest increases in the ST1 wind stress from roughly 5–10 to 50% on 4 and 5 February (the 2 days of highest wind stress). The uncertainties in these new parameterizations, plus the lack of wave measurements at ST1 to be used in the Taylor and Yelland [2001] parameterization, make these comparisons with TC2.5 difficult to assess. On the basis of the comparisons with Hare *et al.* [1999] and Johnson *et al.* [1998], we think that the ST1 wind stress may be underestimated using TC2.5 by up to roughly 10% during this and other major storms during the 1995 GBSS.

[32] The near-bottom oscillatory currents produced by the surface waves during this storm in combination with the tidal currents modified the local bedforms and caused sediment suspension at ST1 [Werner *et al.*, 2003b]. While several other storms contributed to bedform modification, only this nor’easter caused sediment suspension at ST1

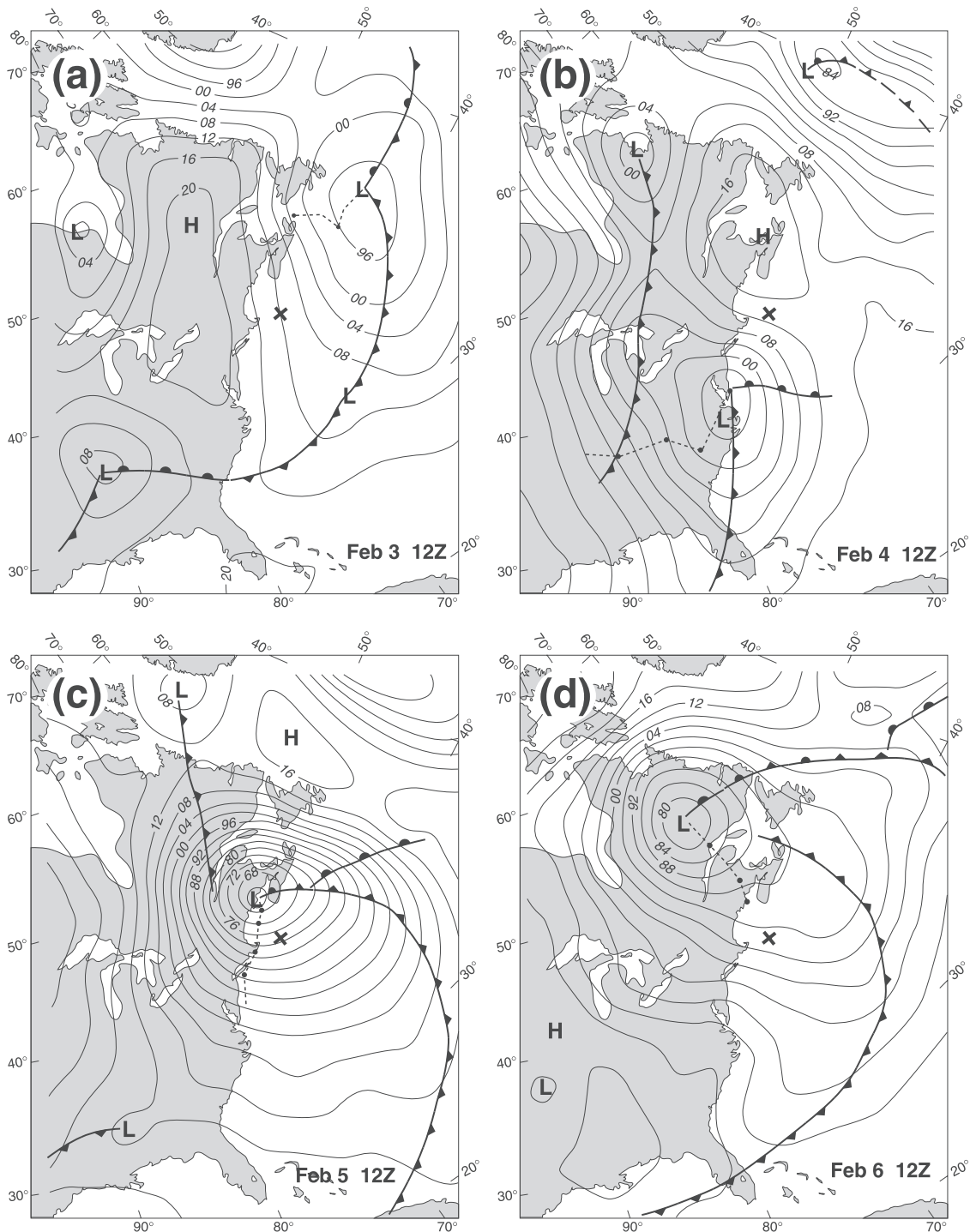


Figure 10. Surface analysis maps for (a) 1200 UT 3 February, (b) 1200 UT 4 February, (c) 1200 UT 5 February, and (d) 1200 UT 6 February. ST1 located at cross ESE of Cape Cod, and tracks of low-pressure systems shown by dashed lines with tick marks every 6 hours from time of map. Isobars are labeled in mbar relative to 1000 mbar (e.g., the label 12 indicates a surface pressure of 1012 mbar, and 90 indicates a pressure of 990 mbar).

during February–April when a bottom camera system was deployed.

5.2. Developing Low Moving Up the St. Lawrence River Valley

[33] On 3 April, a large but weak low-pressure system centered over the Great Lakes moved toward the east and

northeast along the St. Lawrence River valley, arriving near Newfoundland on early 6 April (Figure 13). Characteristic of lows that deepen as they move along this frequent storm track, this storm intensified (with a drop in center pressure from 991 mbar (1800 UT 4 April) to 980 mbar (1200 UT 5 April) to 976 mbar (0600 UT 6 April), a total drop of 15 mbar in 36 hours, and created a strong flow of relatively

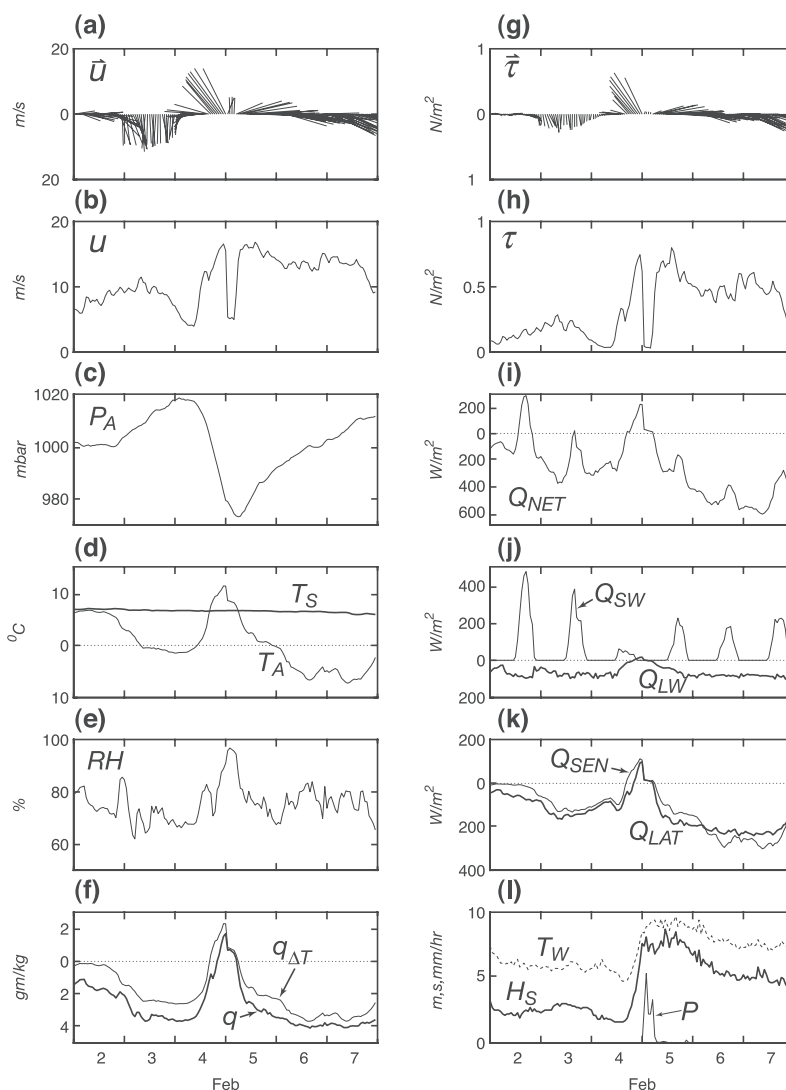


Figure 11. Plot of ST1 (a) wind, (b) wind speed, (c) barometric pressure, (d) air and sea surface temperatures, (e) relative humidity, (f) specific-humidity difference (total (thick line) and that part due to air-sea temperature difference), (g) wind stress, (h) wind stress magnitude, (i) Q_{NET} , (j) Q_{SW} and Q_{LW} , (k) Q_{SEN} and Q_{LAT} , and (l) precipitation (P) and buoy 44011 significant wave height (H_S) and wave period (T_W) for 2–7 February.

dry, subzero air from northern Canada across New England for over 36 hours.

[34] As the barometer fell and winds increased at ST1 on 4 April, warm moist marine air was carried north and eastward, causing a roughly half-day period of surface warming by positive air-sea heat fluxes into the ocean (Figure 14). As soon as the pressure began to rise on 5 April, winds turned to east-southeast, increased in strength, reaching over 15 m/s by nighttime, as cold, dry continental air spread across the Gulf of Maine. Air temperature at ST1 dropped 12°C, leading to an air-sea temperature difference of $T_A - T_S = -5$ to -7°C for a 36-hour period starting about 0800 UT 5 April. This cool air was relatively dry, with $RH \sim 60$ –70%. The strong east-southeast winds, large air-sea temperature difference and low RH all contributed to large latent and sensible heat losses that individually exceeded -100 W/m^2 over much of 5–6 April. These air-sea flux losses combined with long-wave cooling

($Q_{LW} = -80 \text{ W/m}^2$) to produce a net cooling rate of -400 W/m^2 during the night of 5–6 April. The wind stress during this night averaged 0.7 N/m^2 .

[35] By 7 April, winds had greatly diminished, and warm, very humid air returned to Georges Bank. The air-sea temperature difference decreased to $<1^\circ\text{C}$, and thick clouds covered the bank, greatly reducing insolation. The resulting mean surface heat flux for the day was $Q_{NET} \sim 0$, with the weak Q_{SW} (47 W/m^2) offset by Q_{LW} (-22 W/m^2), Q_{LAT} (-20 W/m^2), and Q_{SEN} (-3 W/m^2).

5.3. Spring Lows Moving Up the East Coast From Cape Hatteras

[36] On 1 May, a weak low formed over the southeast United States and started to move eastward toward Cape Hatteras (Figure 15). On 2 May, this low started to deepen as it moved offshore from Cape Hatteras toward the northeast. By 1200 UT 3 May, the center pressure had

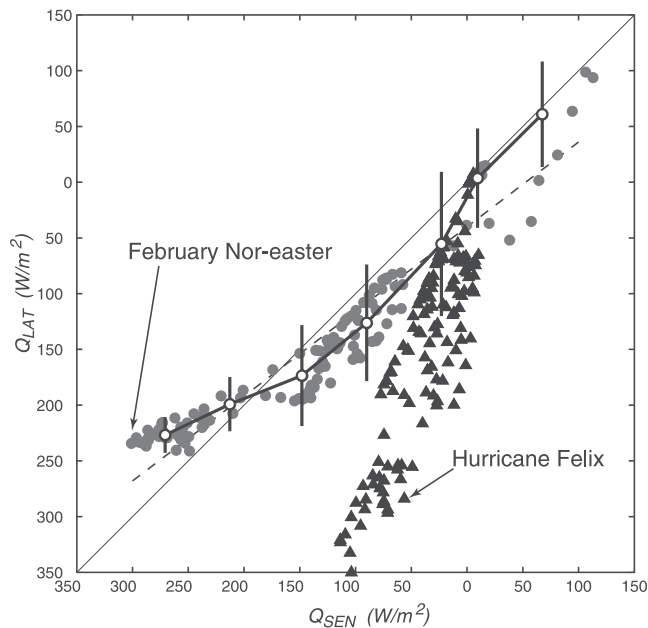


Figure 12. Scatterplot of ST1 Q_{SEN} versus Q_{LAT} for 3–7 February nor'easter (dots) and 18–23 August tropical storm Felix (triangles). Dashed line is least squares linear fit for nor'easter data. Thick solid line connects the mean Q_{SEN} and Q_{LAT} values within seven bins spanning Q_{SEN} computed over the deployment period prior to 18 August when Felix began to influence the bank. The vertical bar plotted at the center of each bin denotes approximate 95% confidence limits. The Bowen ratio is one along the 1:1 diagonal line.

dropped to 992 mbar (an average rate of -0.4 mbar/hr) as the center passed close to the south of Georges Bank. This low, and the slightly weaker low that preceded it 2 days earlier along this same track, brought strong southwest winds to Georges Bank, with peak stresses in excess of 0.5 N/m² on 1 May and 0.8 N/m² on 3 May (Figure 16). These two lows remained small in horizontal scale, so the periods of high winds at ST1 were relatively brief.

[37] Unlike the 4–8 February nor'easter described earlier, these May storms carried relatively warm continental air over the ocean, resulting in much weaker cyclogenesis. At ST1, the air-sea heat fluxes were weak despite the strong winds, with latent cooling (due mostly to the lower RH) partially offset by sensible warming (Figure 16). Both frontal systems brought thick cloud cover and significant precipitation to ST1, especially on 1 May when the daily mean shortwave warming was reduced to 14 W/m² (about 5% of the shortwave heat flux on 4 May, the first clear day after the two storms) and a total of 5.2 cm of rain fell at ST1. The dense cloud cover on this day also cut the net long-wave cooling to 9 W/m², causing the net surface heat flux for the day to be roughly zero. On 3 May, the mean heat flux increased to 59 W/m², as the shortwave component reached 180 W/m², roughly 60% of the shortwave flux on 4 May. On 4 May, after the storm passed, with clear skies and winds below 5 m/s at ST1, the mean net surface flux was 297 W/m². The passage of these two spring storms illustrate the large and rapid changes in surface forcing that can occur on Georges Bank.

5.4. Tropical Storm Felix

[38] Hurricane Felix formed near the Cape Verde Islands on 8 August and developed into a major hurricane (with lowest center pressure of 929 mbar and highest winds about 140 mph (63 m/s) on 12 August) as it moved west and northwest toward the U.S. Atlantic coast. A weakened Felix approached within 240 km of Cape Hatteras on 17 August (center pressure 972 mbar), then moved northeastward, made a clockwise loop toward the southeast (weakening to a tropical storm) before continuing northeast parallel to the coast, passing off Georges Bank on 21 August (center pressure 982 mbar) (Figure 17).

[39] A weak cold front separating Felix and a high over eastern Canada moved southward over Georges Bank on early 18 August. As Felix entrained this cold front cyclonically around its center over the next few days, Felix carried cooler and drier air southeastward across the Bank (Figure 18). This effect is most noticeable on 19 August during the initial pass of Felix, but also occurred on 20–21 August until tropical storm Felix passed northeastward past Newfoundland. With the cold front and passage of Felix came increased cloud cover with the exception of 19 August, when normal insolation was measured at ST1. The passage of Felix brought no precipitation to Georges Bank.

[40] This dying hurricane produced moderate wind stress and strong heat loss at ST1 (Figure 18). The wind stress reached a peak near 0.4 N/m² on 19 August just after the center passed to the east, with only a small increase in sea state to $H_S \sim 4$ – 5 m. The hurricane-driven southwest winds brought cooler, slightly drier air which combined to drive moderate sensible and strong latent heat loss. For 0000–1200 UT 19 August, the mean wind stress was 0.38 N/m², $Q_{NET} = -471$ W/m², the net radiative flux $Q_{SW} + Q_{LW} = -66$ W/m², $Q_{SEN} = -95$ W/m², and $Q_{LAT} = -311$ W/m². The maximum latent loss ($Q_{LAT} = -372$ W/m²) occurred near 0800 UT 19 August. About 80% of this large latent heat flux was due to two factors, the large air-sea temperature difference ($T_A - T_S = -4.8^\circ\text{C}$) and high mean temperature (mean $(T_A + T_S) = 21.7^\circ\text{C}$), which allows the air-sea specific-humidity difference to be large. Only about 20% of the latent flux was due to the small decrease in RH as the hurricane carried slightly drier air over Georges Bank. During the 3-day period 18–20 August, sensible and latent fluxes were roughly linearly correlated ($r^2 = 0.83$), with $Q_{LAT} = (-35 \pm 28) + (2.96 \pm 0.33) \times Q_{SEN}$. Note that the Bowen ratio $B = Q_{LAT}/Q_{SEN} \approx 3.0 \pm 0.3$ was quite different from that found during the winter storm (Figure 12).

6. Comparison of ST1 and CR Air-Sea Heat Fluxes

[41] Water over the crest of Georges Bank (within the tidal mixing front) is kept vertically well mixed throughout the year by vigorous tidal dissipation [Flagg, 1987]. As the seasonal thermocline develops over the southern flank at ST1, the surface temperature there becomes warmer than over the crest, where the deeper mixing slows the rate of increase in surface temperature. In this section, we use air and sea surface temperature measurements made at the crest mooring site CR to estimate the air-sea heat fluxes there, and examine if the on-bank change in T_S from ST1 to CR causes significant spatial changes in these fluxes. Q_{SEN} and

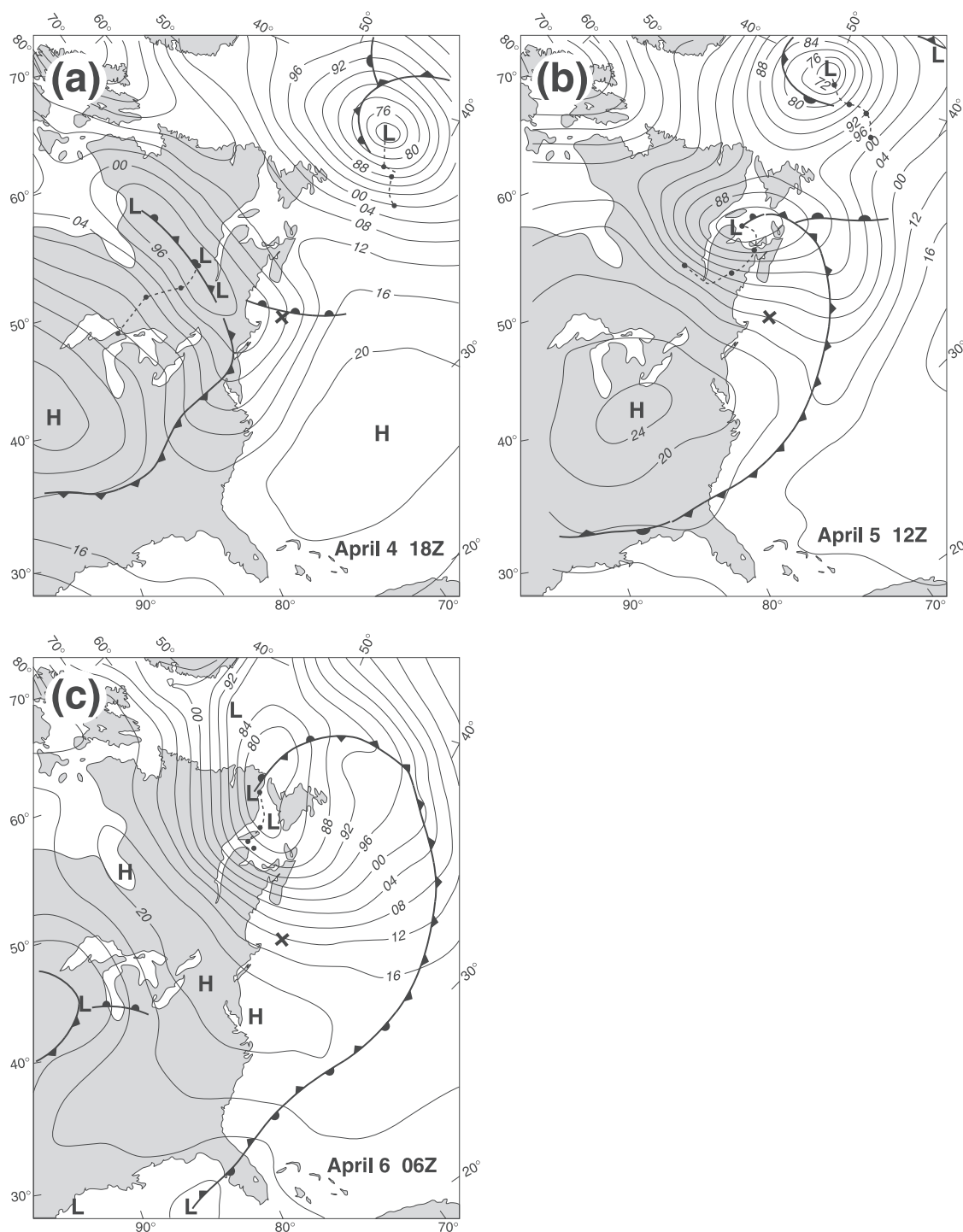


Figure 13. Surface analysis maps for (a) 1800 UT 4 April, (b) 1200 UT 5 April, and (c) 0600 UT 6 April. As in Figure 10, ST1 location shown by cross, storm tracks shown by dashed lines with tick marks every 6 hours, and isobars labeled relative to 1000 mbar.

Q_{LAT} are computed using the CR T_A and T_S and the wind speed and RH measured at ST1, under the assumption that the wind speed and RH vary little over the 60 km separating the two sites.

[42] Air temperatures at ST1 and CR tend to track closely before about 1 July, with a mean difference of only 0.1°C and standard deviation of 0.9°C . During this initial period, sea surface temperatures at ST1 and CR also tracked

closely, with a mean difference of 0.1°C and standard deviation of 0.9°C (Figure 19). After 1 July, the surface temperature at ST1 became noticeably warmer than at CR as the shallow thermocline continued to develop over the southern flank, and, in August, the shelf-slope front moved on-bank during a large intrusion of warmer slope water over the southern flank. This intrusion caused the surface temperature to increase, reaching a maximum of 25.5°C at ST1,

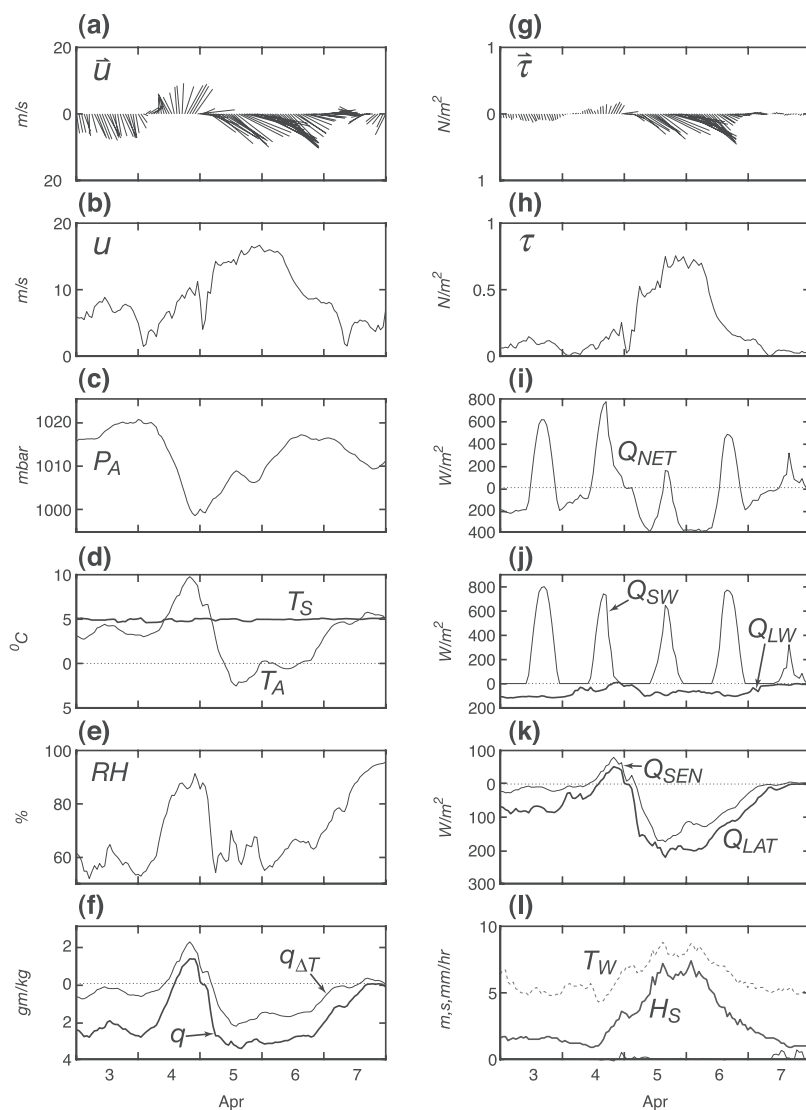


Figure 14. Plot of ST1 surface conditions and fluxes for 3–7 April. Format same as Figure 11.

6°C warmer than at CR, on 17 August (see Churchill *et al.* [2003] for a detailed description of this and other slope water intrusions observed over the southern flank during 1995). From 1 July to the end of the deployment, the air temperature at ST1 was warmer than at CR on average by $2.1 \pm 1.6^\circ\text{C}$, and the sea surface temperature by $3.2 \pm 2.1^\circ\text{C}$.

[43] This large difference in surface temperature between CR and ST1 (ΔT_S) leads to a marked difference in the air-sea heat fluxes, especially during the August slope water intrusion when tropical storm Felix brought high winds and relatively cooler air over Georges Bank (Figure 19). In August, T_A was always slightly warmer than T_S at CR, resulting in weak sensible heating and small positive and negative latent fluxes there (Figure 19). At ST1, modest sensible and large latent cooling occurred due to the large negative air-sea temperature differences there. From 1 July to the end of the deployment, the mean ST1-CR differences in Q_{SEN} and Q_{LAT} were $-10 \pm 21 \text{ W/m}^2$ and $-23 \pm 53 \text{ W/m}^2$, respectively, with the largest difference in Q_{LAT} being -300 W/m^2 on 19 August. (The large ST1-CR T_S difference in late summer also leads to a modest difference in the infrared radiation emitted by the ocean surface. To lowest

order, the ST1-CR difference in upward long-wave flux is $\Delta Q_{LW\uparrow} = 5.5 \Delta T_S$, such that the July–August mean difference of $\Delta T_S = 3.2^\circ\text{C}$ produces a $\Delta Q_{LW\uparrow} = 18 \text{ W/m}^2$. The impact of this modest difference on the net long-wave flux is not clear, since the amount of downward long-wave radiation at CR might be expected to decrease due to the cooler air there.)

[44] These air-sea heat flux estimates suggest the following picture. During winter and early spring, the air-sea heat flux ($Q_{SEN} + Q_{LAT}$) into the southern flank and crest waters is essentially spatially uniform. As the surface waters over the southern flank become warmer than over the crest in summer, the temperature of the air just above the surface tends to adjust to this pattern, so that the resultant air-sea heat flux into the ocean is on average positive and relatively small, with slightly more heat flux (of order 10 W/m^2 or less) into the cooler crest water. During August 1995, two events modified this picture. First, a large slope water intrusion carried warmer surface water over the southern flank, which led to sensible cooling over this warmer surface. Second, the passage of a tropical storm south of Georges Bank brought high winds and cold air over the bank, leading to large air-sea cooling, especially over the slope water intrusion.

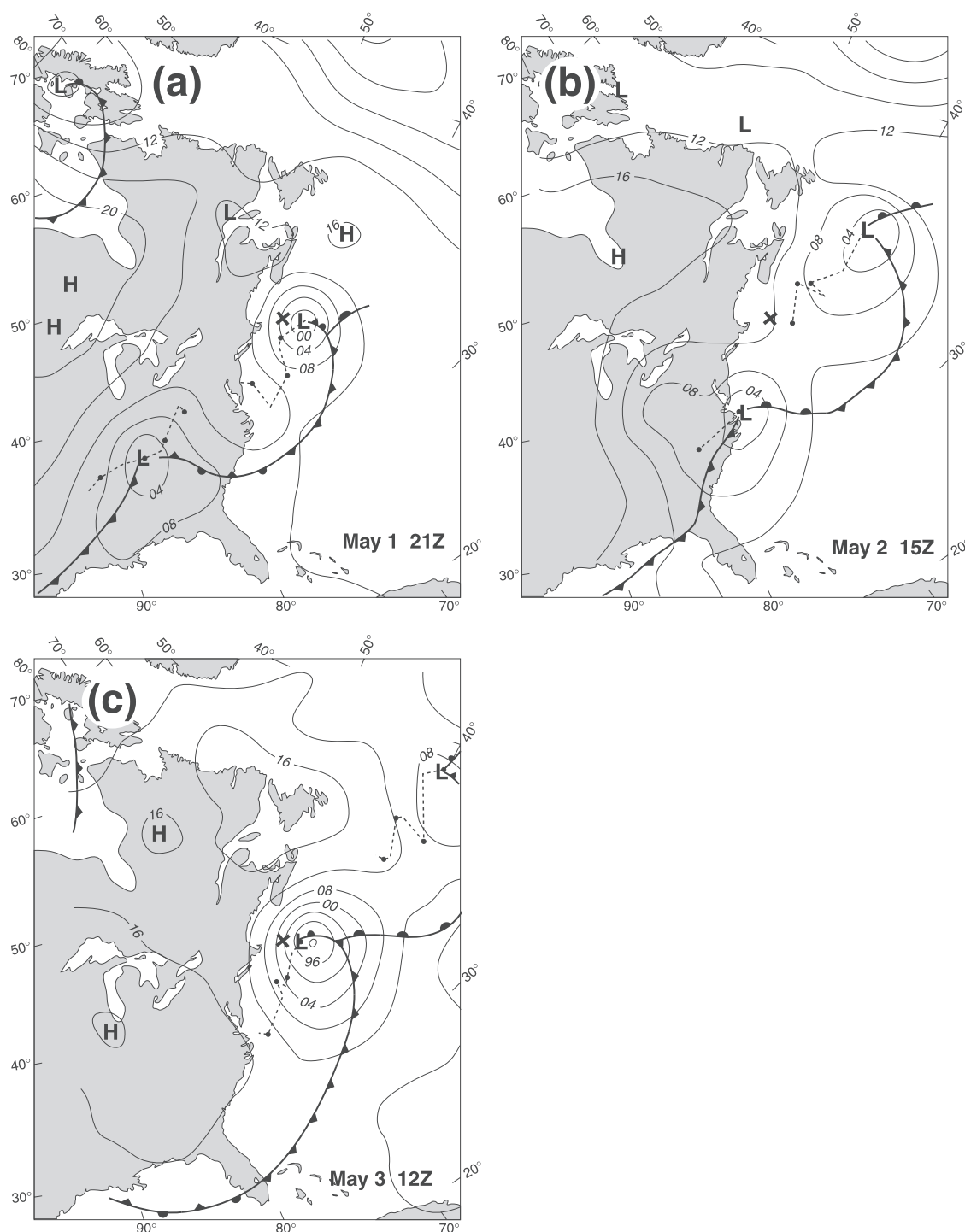


Figure 15. Surface analysis maps for (a) 2100 UT 1 May, (b) 1500 UT 2 May, and (c) 1200 UT 3 May. As in Figure 10, ST1 location shown by cross, storm tracks shown by dashed lines with tick marks every 6 hours, and isobars labeled relative to 1000 mbar.

[45] The effect of the summer on-bank T_S difference on the radiative heat flux components is not clear. The cooler T_S over the crest reduces the upward flux of long-wave radiation, but the frequent presence of fog over the cool crest may (1) reduce the net shortwave heating, and (2) reduce the net long-wave cooling by re-radiating more of the upward long-wave radiation back toward the ocean surface. This negative feedback has been observed in other coastal environments (e.g., off northern California [Beardsley *et al.*,

1998]) and should tend to reduce the net effect of fog on the total radiation flux.

7. Climatology

[46] The surface wind stress and heat flux measured at ST1 during the 1995 GBSS show clear fluctuations on monthly and longer timescales. In this section, we first address the question of whether the surface forcing on

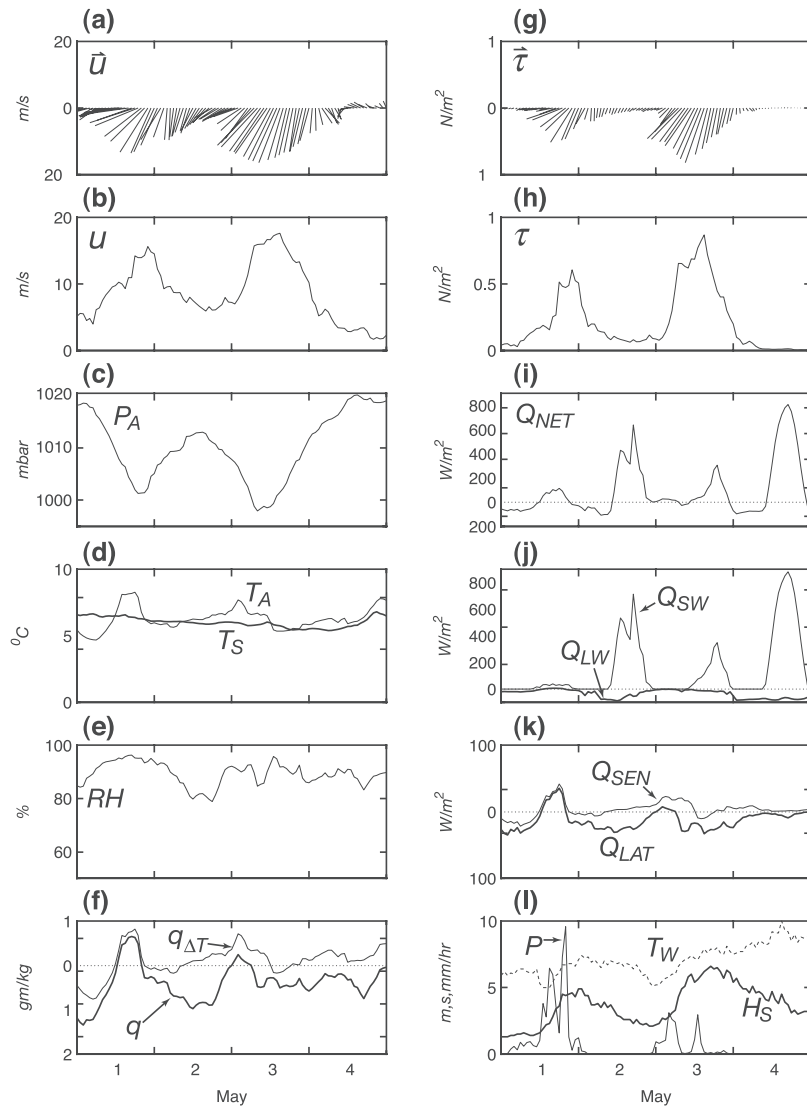


Figure 16. Plot of ST1 surface conditions and fluxes for 1–3 May. Format same as Figure 11.

Georges Bank during 1995 was “typical”, i.e., within the range of fluctuations observed over a span of many years. The analyses of two long time series, the 1984–1999 NDBC buoy 44011 wind data and the 1974–2001 daily insolation in Woods Hole, Massachusetts (Figure 1), suggest that the surface conditions over the bank during 1995 were well within local interannual variations. We then compare the ST1 surface heat flux with the monthly SOC surface flux climatology (described in section 2) to assess the accuracy of this ship-based product on the southern flank of Georges Bank.

7.1. Interannual Variability

[47] To compare variability on monthly and longer time-scales, monthly mean values of the wind stress variance ($\tau_x^2 + \tau_y^2$) were computed using the 1984–1999 buoy 44011 wind time series and plotted in Figure 20 with the 1995 values highlighted. Despite numerous gaps in the record, Figure 20 suggests that 1995 was a normal year and that there is no clear many-year trend in variability. Based on this, we then computed the mean and 95% confidence

limits for each month (using the buoy 44011 time series without 1995). Figure 21 compares the 1995 monthly mean values plotted with these long-term means. The 1995 values for all months lie near the long-term means, well within the confidence limits. This supports the visual conclusion from Figure 20 that the wind stress variability at buoy 44011 on eastern Georges Bank during the 1995 GBSS was typical and not an extreme. A similar analysis of the 1984–1999 monthly mean air and sea surface temperatures at buoy 44011 shows that the 1995 February through August monthly mean values were also typical and within the 95% confidence estimates, even though the 1995 August mean sea surface temperature was 22.6°C, 4.1°C above the long-term August mean, due to a pronounced warm slope water intrusion over the southern flank [see Churchill *et al.*, 2003].

[48] R. Payne (WHOI) has used Eppley pyranometers mounted on the roofs of the WHOI Smith and Clark Laboratories to collect a unique, nearly continuous record of daily insolation over land in Woods Hole starting in 1974. A plot of the monthly mean insolation time series

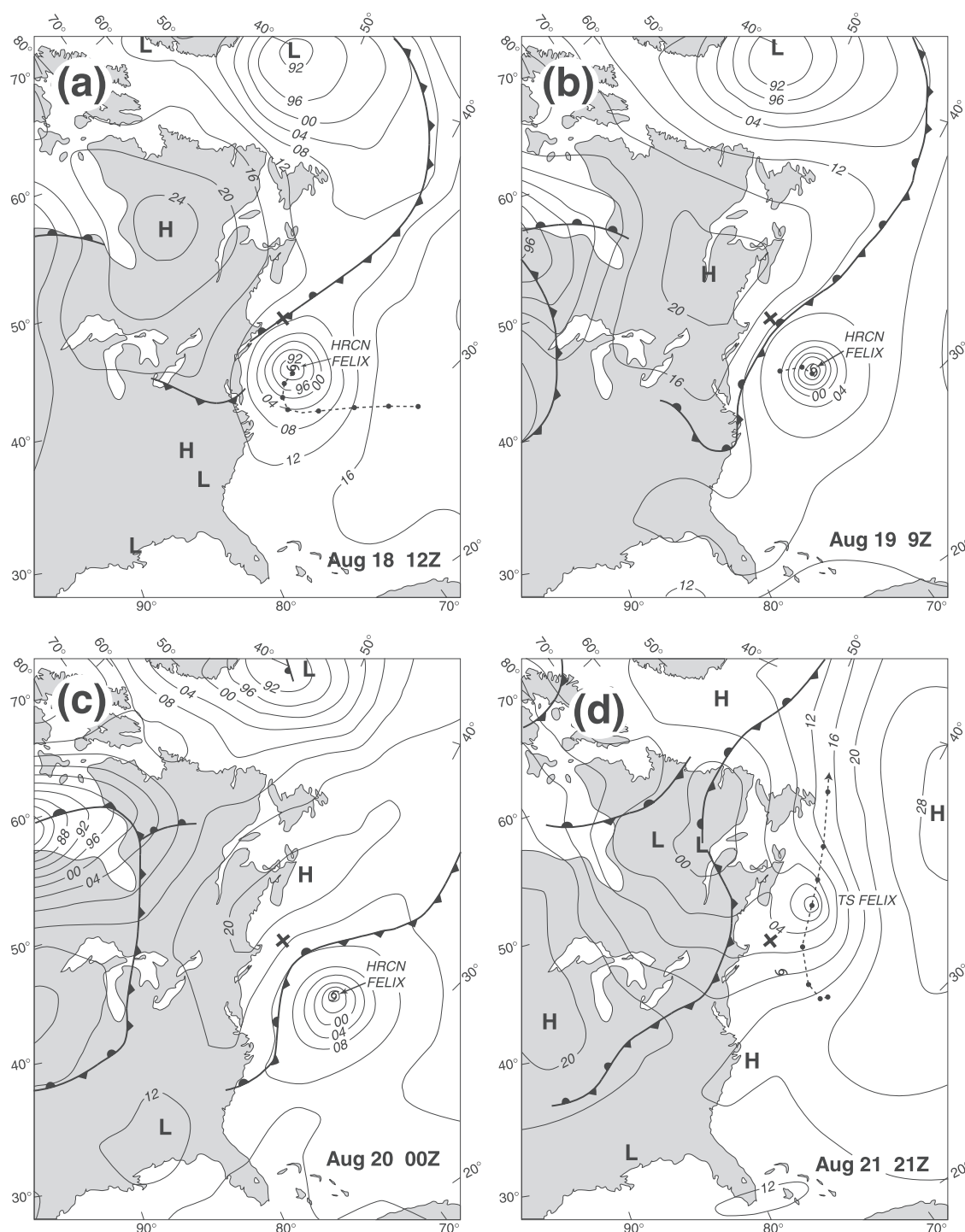


Figure 17. Surface analysis maps for (a) 1200 UT 18 August, (b) 0900 UT 19 August, (c) 0000 UT 20 August, and (d) 2100 UT 21 August. ST1 location shown by cross, the track of hurricane and tropical storm Felix shown by the dashed line with tick marks every 12 hours, and isobars labeled as in Figure 10.

with the 1995 values highlighted (Figure 20) suggests that 1995 was also a typical year for insolation in Woods Hole. The comparison of the 1995 WHOI values with the monthly means and 95% confidence limits computed using the 1974–2001 record (without 1995) (Figure 21) indicates some differences during the February–August period, especially with August 1995 being 35 W/m^2 higher than the long-term mean, just at the upper confidence limit, but

all other monthly values for 1995 are within the 95% confidence limits. It seems plausible that this result also applies to the insolation measured at ST1 during 1995. Daily mean insolation at ST1 and WHOI are clearly correlated, with a decorrelation timescale of roughly 1.5 days; however, the ST1 record is too short to determine if variations on timescales of weeks and longer are similar at the two sites. Over the 101-day 1995 summer analysis period, the mean

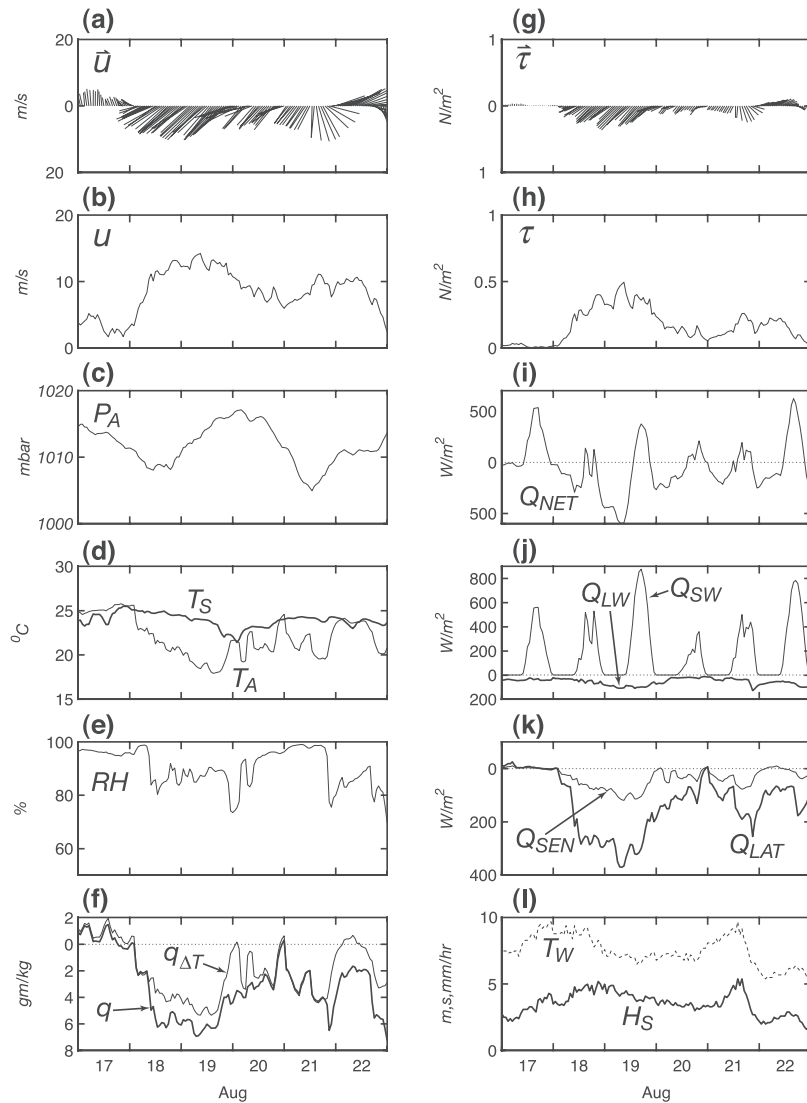


Figure 18. Plot of ST1 surface conditions and fluxes for 17–22 August, following Figure 11 format. There was no measurable precipitation at ST1 during this period.

difference in daily insolation was $4 \pm 71 \text{ W/m}^2$, only 1.6% of the mean insolation of 252 W/m^2 observed at ST1, suggesting that on these long timescales, insolation at WHOI and ST1 agree to within measurement uncertainty. (This is not true on shorter timescales of a few days to several weeks. The spectrum of daily mean insolation has significant energy (roughly 45% of the total) at periods greater than 10 days, which prevents accurate prediction of daily mean insolation at ST1 using WHOI insolation.)

7.2. ST1-SOC Heat Flux Comparison

[49] The SOC surface flux climatology represents a spatial and temporal average of surface flux components computed using ship meteorological reports and bulk formula [Josey *et al.*, 1998]. Ship data collected from 1980 through 1994 are included, and mean values computed for each one degree latitude/longitude box. Due to the topography of Georges Bank, we consider here two boxes for comparison with ST1, the “southern flank” box ($40^\circ\text{--}41^\circ\text{N}$, $67^\circ\text{--}68^\circ\text{W}$) and a “crest” box ($41^\circ\text{--}42^\circ\text{N}$, $67^\circ\text{--}68^\circ\text{W}$). The southern flank box includes ST1 but extends southward over the continental

slope, so that the surface fluxes will reflect both those over the shelf and slope. The crest box covers much of the crest with little extension into the Gulf of Maine, so its fluxes should be representative of the crest itself. Comparison of the SOC heat flux values for these two boxes (Figure 21) shows nearly identical seasonal variations, but with enhanced latent cooling on average (31 W/m^2) over the southern flank relative to the crest. This spatial difference causes the net heat flux to be -20 W/m^2 over the southern flank, and $+18 \text{ W/m}^2$ over the crest (Table 5).

[50] The monthly ST1 heat flux components exhibit similar seasonal variation with the SOC data, but with clear differences (Figure 21). With the notable exception of August, the latent, long-wave, and sensible cooling at ST1 were less than the SOC values in both boxes (Table 5). Over the entire 8-month deployment period, the mean ST1 Q_{LAT} loss was 40 W/m^2 and 11 W/m^2 less than the southern flank and crest SOC values. This difference, plus a smaller but consistent difference in net long-wave cooling, results in the ST1 net heat flux being 55 W/m^2 and 19 W/m^2 larger than SOC. The enhanced latent and long-wave cooling at ST1 in

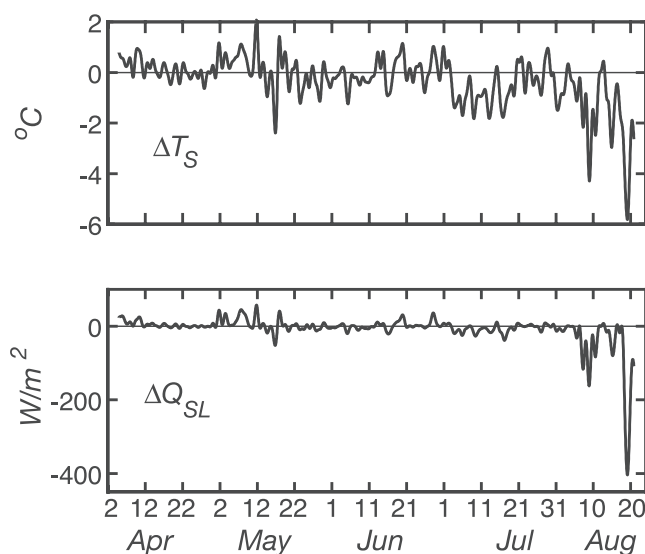


Figure 19. (top) Low-passed time series of crest (CR) minus southern flank (ST1) sea surface temperature difference (ΔT_S) and (bottom) combined sensible and latent heat flux difference (ΔQ_{SL}).

August is due to the strong storm in early August and Hurricane Felix (Figure 6).

[51] A recent comparison between the SOC surface flux climatology and buoy heat flux data collected in the eastern North Atlantic shows the two net heat flux to agree to within 10 W/m^2 [Josey, 2001]. While our comparison at ST1 on Georges Bank is more limited (only one versus five buoys and seven months versus two year deployments), Figure 21 does suggest a bias of order $10\text{--}40 \text{ W/m}^2$ in the SOC latent cooling, which contributes to a slightly larger bias of order $20\text{--}60 \text{ W/m}^2$ in net surface cooling. Whether this is a true systematic bias or an artifact of small sample size in the ST1 comparison data set or the SOC ship data

density is not known. Josey [2001] concludes that despite the excellent agreement found in the eastern North Atlantic comparison, the SOC climatology must contain some areas with strong biases; our data suggests that some bias does exist over Georges Bank.

7.3. Precipitation

[52] The monthly mean precipitation P at ST1 and two coastal stations on Cape Cod (Edgartown on Martha's Vineyard, and Hatchville near Woods Hole) varied significantly during spring-summer 1995 (Table 6). Long-term records at these two coastal stations exhibit a weak seasonal cycle, with a maximum in $P \sim 10.2 \text{ cm/month}$ in April and a minimum of $\sim 7.6 \text{ cm/month}$ in July. During February through May 1995, the monthly precipitation at ST1 exceeded that on Cape Cod, with the four-month average P at ST1 (10.7 cm/month) larger by a factor of 1.5 than the mean measured coastal precipitation (7.1 cm/month). The seasonal mean during this period was 9.8 cm/month , indicating that the late winter/spring 1995 was drier than normal on Cape Cod. During June through August, mean precipitation at ST1 decreased below the seasonal cycle at the two Cape stations, and while P at ST1 and Hatchville varied in rough agreement (within 20%), P at Edgartown differed in June and August by roughly +70% and -65% in comparison to ST1. While the total precipitation measured on Georges Bank at ST1 during 1995 exceeded by $\sim 21\%$ that measured at two representative stations on Cape Cod, roughly 230 km WNW of ST1, the highly episodic nature of precipitation and the shortness of the ST1 record combine to prevent drawing any conclusions about the predictability of precipitation on Georges Bank using land-based data on Cape Cod.

8. Summary

[53] A moored array of meteorological and oceanographic instrumentation was deployed on Georges Bank during February–August 1995 as part of the U.S. GLOBEC

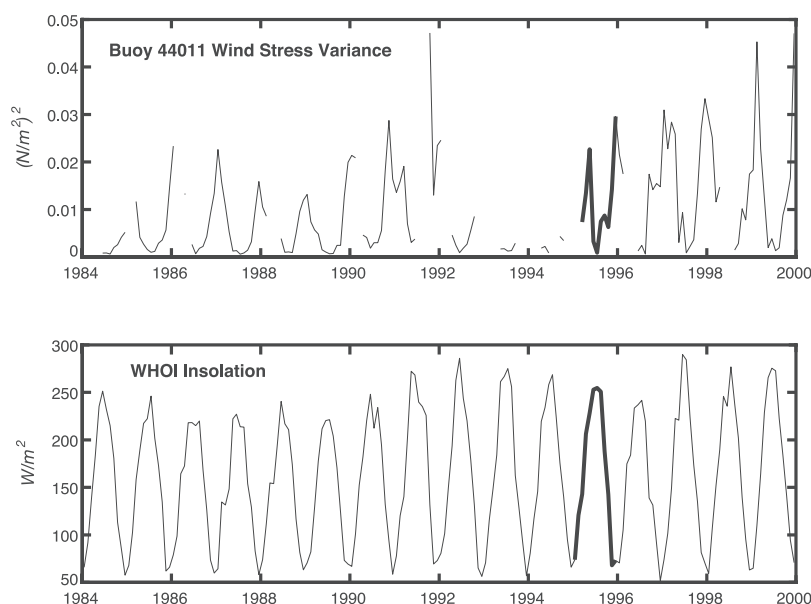


Figure 20. (top) Monthly mean wind stress variability at buoy 44011 and (bottom) insolation at WHOI for 1984–1999, with 1995 values highlighted.

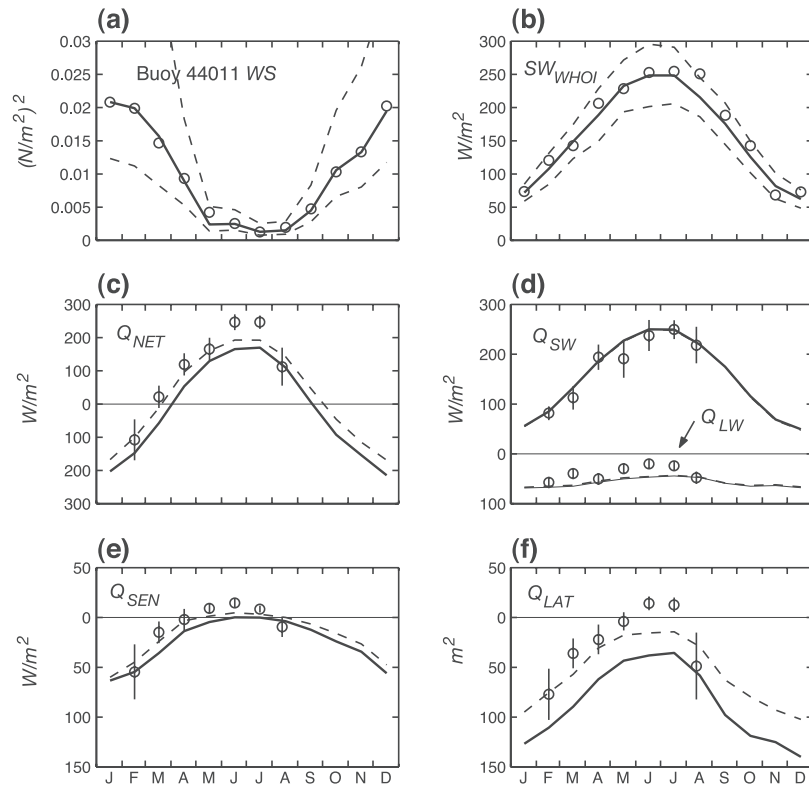


Figure 21. Comparison of 1995 data with climatology: (a) wind stress variance at buoy 44011; (b) WHOI insolation; (c) Q_{NET} ; (d) Q_{SW} and Q_{LW} ; (e) Q_{SEN} ; and (f) Q_{LAT} . In all panels, the 1995 monthly values are shown as circles. In Figures 21a and 21b, climatologically monthly mean and 95% confidence limits are shown as solid and dashed lines. In Figures 21c–21f, ST1 data also shown with approximate 95% confidence limits (denoted by the vertical line through each circle), and SOC values for southern flank and crest boxes shown as solid and dashed lines. Note changes in vertical scales.

NW Atlantic/Georges Bank Stratification Study. One primary objective of this array was to investigate the role of surface forcing on the onset and evolution of seasonal stratification over the southern flank. Winds, air temperature, relative humidity, barometric pressure, incident short- and long-wave radiation, precipitation, and near-surface ocean temperature and currents were measured at the central southern flank site ST1, located on the 76-m isobath, roughly halfway between the tidal mixing and shelf/slope fronts. After filling a gap in the ST1 winds using wind data from NDBC buoy 44011 located on eastern Georges Bank, the surface momentum, heat, and moisture fluxes at ST1 were computed using the TOGA/COARE (version 2.5) bulk formulation. Air and sea surface temperature measurements made at a crest site allowed estimation of some heat flux components there for spatial comparison.

[54] The surface wind stress variability at ST1 was dominated by a succession of atmospheric low-pressure systems that pass Georges Bank during the deployment period. A transition between frequent lows and strong wind stress events (“winter”) to less frequent lows and weaker wind stress events (“summer”) occurred in mid-May. In winter, wind stress fluctuations tended to be omnidirectional with an average magnitude of 0.13 N/m^2 , with maximum stresses above 0.5 N/m^2 during four storms, one a classic “nor’easter.” In summer, wind stress fluctuations were weaker (average magnitude 0.05 N/m^2) but more strongly polarized, with the major axis aligned roughly parallel with

the southern flank isobaths. The strongest wind stresses in summer were associated with the passage of tropical storm Felix south of Georges Bank in August.

[55] The surface heat flux at ST1 and its variability were dominated by shortwave heating. The deployment period started before the spring equinox and ended after summer solstice, so both the diurnal day/night variation and large seasonal increase in insolation were captured. Shortwave heating increased from a winter mean of about 130 W/m^2 to 230 W/m^2 in summer. Mean long-wave cooling decreased from about -50 W/m^2 in winter to -30 W/m^2 in summer, with an increased downward flux due to warmer, more-moist overlying air overcompensating for the increased

Table 5. ST1 and SOC Heat Flux Comparison^a

Deployment	Q_{NET}	Q_{SW}	Q_{LW}	Q_{SEN}	Q_{LAT}
	<i>Mean</i>				
ST1	115	183	-39	-7	-23
SF	60	193	-54	-16	-62
CR	96	192	-52	-9	-34
ST1-SF	55	-9	15	9	40
ST1-CR	19	-8	14	2	11
	<i>Annual Mean</i>				
SF	-20	151	-59	-25	-87
CR	18	150	-57	-18	-56
SF-CR	-38	1	-1	-7	-31

^aSOC southern flank and crest boxes are denoted SF and CR. Units: W/m^2 .

Table 6. Monthly Mean Precipitation P , Evaporation E , and $P + E$ at ST1, Plus Monthly Mean P at Edgartown, Hatchville, and Boston, Massachusetts^a

Month	ST1 P	ST1 E	ST1 $P + E$	Hatchville P		Edgartown P		Boston P_M	
February	7.5	-7.3	0.2	4.7	(9.3)	4.3	(9.2)	6.5	(9.2)
March	13.9	-3.8	10.1	6.8	(9.8)	6.9	(10.0)	5.6	(9.4)
April	7.9	-2.2	5.7	7.0	(10.2)	5.5	(10.3)	3.6	(9.1)
May	13.6	-0.4	13.2	9.1	(9.5)	12.5	(10.2)	4.6	(8.3)
June	7.7	1.4	9.1	8.2	(9.2)	13.0	(8.5)	3.9	(7.8)
July	5.6	1.3	7.0	6.6	(7.9)	8.9	(7.4)	5.2	(7.2)
August ^b	6.8	-3.9	2.9	8.0	(8.8)	2.4	(9.1)	2.1	(8.2)
Total	63.0	-14.8	48.2	50.5	(64.7)	53.7	(64.8)	31.5	(59.3)

^aMonthly values for 1995 are listed first, followed by the long-term (30-year) mean monthly precipitation in parenthesis for the coastal stations. Coastal data from *National Oceanic and Atmospheric Administration* [1995a, 1995b]. Boston is included for reference, but was even drier during 1995 than Cape Cod, and not expected to provide a good predictor of precipitation on Georges Bank. All values in cm.

^bThe ST1 precipitation record ended on 23 August when the mooring was recovered. No precipitation was recorded at Hatchville and Edgartown and only 0.08 cm at Boston for the rest of August, so that we can consider that the total precipitation measured during the first 23 days at ST1 is a good estimate of the total August precipitation.

upward flux due to warmer ocean surface temperature in summer. Sensible and latent heat fluxes were more negative (ocean cooling) and variable in winter, due to larger air-sea temperature and specific humidity differences and winds associated with passing lows. These fluxes were weaker and weakly positive in summer, due to warmer air overlying cooler water. The winter (summer) mean sensible and latent fluxes were roughly -20 ($+10$) W/m^2 and -40 (0) W/m^2 respectively. Overall, winter was characterized by weak net heating (30 W/m^2) with shortwave gain offset by long-wave, latent, and sensible heat loss. In summer, increased shortwave gain and reduced long-wave loss and weak sensible and latent fluxes combined to produce strong net heating (210 W/m^2).

[56] Precipitation at ST1 was highly episodic, with heavy rains occurring only 7 times during the eight-month deployment, contributing roughly 60% of the total precipitation. Consistent with coastal records, monthly mean precipitation at ST1 was more constant, exhibiting little seasonal change. Evaporation at ST1 occurred mostly during winter, associated with lows advecting cold, dry continental air across the bank. Over the deployment period, the net evaporation was roughly -15 cm, giving a net freshwater flux of $+48$ cm.

[57] Comparison of wind stress at NDBC buoy 44011 during 1995 with wind stress there for 1984–1999 indicates that wind stress variability over Georges Bank during the 1995 Stratification Study was typical and not an extreme. Comparison of the monthly ST1 heat flux with the ship-based Southampton Oceanography Center surface heat flux climatology for the $1^\circ \times 1^\circ$ box on the southern flank suggests that this climatology overpredicts latent cooling by roughly 40 W/m^2 , so that the predicted net positive heat flux is reduced by roughly 50 W/m^2 , with smaller contributions from the other components. The cause of this difference is not known, although part of the difference may be due to overestimation of the true wind from the ship data. COADS wind stress variances are roughly twice as large as those for NDBC buoy 44011.

[58] Analysis of the moored oceanographic plus drifter measurements made during the 1995 Stratification Study show the importance of local surface forcing on currents, water structure and mixing over the southern flank. The reader is referred to other papers in this special section for

detailed descriptions of the ocean response to the surface forcing measured at ST1.

Appendix A: Sea-State-Dependent Surface Roughness

[59] It has long been recognized that the surface roughness and thereby the drag of the ocean on the atmosphere is a function of sea state. The general consensus is that younger (i.e., developing) and/or steeper waves provide more aerodynamic drag, which enhances the momentum transfer across the air-sea interface. *Hare et al.* [1999] proposed a modification to the TOGA/COARE version 2.5 algorithm (TC2.5) that involves a wind speed dependent *Charnock* parameter above 10 m/s to provide better agreement with the larger observed values of the drag coefficient at high winds. This modification constitutes one of the main changes to the TOGA/COARE algorithms now found in TC2.6. Over the open ocean, the youngest seas are normally associated with high wind conditions where the wind-driven waves can fully replace the old sea. The higher probability of young seas on the open ocean under high wind conditions may partially explain the observed drag coefficients. Numerous other investigations have attempted to account for the enhanced transfer over developing seas and/or steep wave by formulating sea-state-dependent roughness parameterizations. For example, *Johnson et al.* [1998] combined recent measurements off the coast of Denmark with the results from *Donelan* [1990] and *Donelan et al.* [1993] to develop a wave-age dependent *Charnock* parameter that predicts that drag will be most enhanced during rapid increases in wind speed when the wave field is developing. Recently, *Taylor and Yelland* [2001] developed a parameterization for sea surface roughness as a function of wave height and wave steepness that shows similar tendencies to the *Johnson et al.* [1998] parameterization.

[60] To examine how these sea-state parameterizations would change the ST1 wind stress time series presented in this paper, we compare here the drag coefficients computed using the *Hare et al.* [1999], *Johnson et al.* [1998], and *Taylor and Yelland* [2001] parameterizations with TC2.5 values for the strong wind stress events described in section 5. Table A1 presents the ratio of the sea-state-dependent drag coefficients to TC2.5 averaged over each

Table A1. Ratio of Recently Proposed Drag Coefficient Parameterizations Compared to the TC2.5 Drag Coefficient Using in This Paper^a

Period	<i>Hare et al.</i> [1999]	<i>Johnson et al.</i> [1998]	<i>Taylor and Yelland</i> [2001]
3 February	1.00	0.97	1.26
4 February	1.03	1.04	1.12
5 February	1.08	1.00	1.46
4 April	1.00	0.96	0.99
5 April	1.07	1.08	1.36
6 April	1.05	0.98	1.21
2 May	1.00	0.89	1.08
3 May	1.08	1.08	1.46
4 May	1.00	0.95	1.14
17 August	1.00	0.96	0.97
18 August	1.02	0.90	0.87
19 August	1.05	1.00	1.16

^aThe ratio represents daily averages. The first column provides the days over which the ratio is averaged. The other columns provide the source of each parameterization.

day to illustrate the change during each event. *Hare et al.* [1999] predicts enhancements of up to 8% during the highest winds during the February nor'easter and the May low, while *Johnson et al.* [1998] tends to predict lower drag during the early ("older" wave) phase of these events and larger drag during the "younger" wave phase. *Taylor and Yelland* [2001] exhibits substantially larger enhancement and greater variability in the drag coefficient. These results suggest that the uncertainty in the ST1 wind stress estimates at high winds due to differences in the parameterizations is approximately 10% if we consider either *Hare et al.* [1999] or *Johnson et al.* [1998]. Consideration of the *Taylor and Yelland* [2001] parameterization suggests an uncertainty closer to 50% at higher winds. The wave age and wave steepness data used in the *Johnson et al.* [1998] and *Taylor and Yelland* [2001] calculations were obtained at NDBC buoy 44011 and not at ST1, and while we think the wave fields should be similar at these two sites, there will be some difference, so that the ratios in Table A1 must be viewed as approximate.

[61] **Acknowledgments.** The 1995 Georges Bank Stratification Study moored array component proved to be a great success, made possible by the skill and support of many individuals working toward a common goal. We want to especially acknowledge B. Way (WHOI Upper Ocean Processes Group), R. Trask (WHOI Rigging Shop), and P. O'Malley and S. Kery (WHOI AOPE Mooring Group) and their coworkers for their leading roles in obtaining the moored surface measurements presented here. We also want to acknowledge the expert support of the captains and crews of the research vessels *Endeavor* and *Seward Johnson*. J. Manning (NMFS) kindly supplied the 1984–1999 buoy 44011 wind stress time series, and R. Payne (WHOI) the long-term WHOI insolation record. C. Alessi, W. Williams, and M. Caruso helped with data processing, and A.-M. Michael and J. Cook helped with final manuscript and figure preparation. Feedback from A. Plueddemann, H. Burchard, and one anonymous reviewer helped improve this presentation. The U.S. GLOBEC Northwest Atlantic/Georges Bank program is jointly funded by the National Science Foundation - Division of Ocean Sciences (NSF) and the NOAA National Marine Fisheries Service (NMFS). The 1995 Stratification Study moored surface measurement program was supported by NSF grants OCE 93-13671 (ST1) and OCE 93-13670 (CR), and subsequent analysis and preparation of this paper was funded through NSF grants OCE 98-06379, 98-06445, and 02-27679. This is WHOI contribution number 10654 and U.S. GLOBEC contribution number 372.

References

Alessi, C., et al., The 1995 Georges Bank Stratification Study moored array measurements, *Tech. Rep. WHOI-01-11*, 101 pp., Woods Hole Oceanogr.

- Inst., Woods Hole, Mass., 2001. (Available at <http://globec.whoi.edu/globec-dir/reports/WHOI-01-11-GLOBEC.pdf>).
- Beardsley, R. C., A comparison of the VACM and new EG&G VMCM on a surface mooring in CODE-1, *J. Geophys. Res.*, **92**, 1845–1859, 1987.
- Beardsley, R. C., A. G. Enriquez, C. A. Friehe, and C. A. Alessi, Intercomparison of aircraft and buoy measurements of wind and wind stress during SMILE, *J. Atmos. Oceanic Technol.*, **14**, 969–977, 1997.
- Beardsley, R. C., E. P. Dever, S. J. Lentz, and J. P. Dean, Surface heat flux variability over the northern California shelf, *J. Geophys. Res.*, **103**, 21,553–21,586, 1998.
- Bigelow, H. B., Physical oceanography of the Gulf of Maine, *U.S. Fish. Bull.*, **40**, 511–1027, 1927.
- Bluestein, H. B., *Synoptic-Dynamic Meteorology in Mid-latitudes*, vol. II, *Observations and Theory of Weather Systems*, 594 pp., Oxford Univ. Press, New York, 1993.
- Brink, K. H., R. Limeburner, and R. C. Beardsley, Properties of flow and pressure over Georges Bank as observed with near-surface drifters, *J. Geophys. Res.*, **108**(C11), 8001, doi:10.1029/2001JC001019, in press, 2003.
- Buckley, L. J., and G. Lough, Recent growth, biochemical composition, and prey field of larval haddock (*Melogrammus aeglefinus*) and Atlantic cod (*Gadus morhua*) on Georges Bank, *Can. J. Fish. Aquatic Sci.*, **44**, 14–25, 1987.
- Bunker, A. F., Computation of surface energy flux and annual air-sea interaction cycles of the North Atlantic Ocean, *Mon. Weather Rev.*, **104**, 1122–1139, 1976.
- Butman, B., and R. C. Beardsley, Long-term observations on the southern flank of Georges Bank. Part I: A description of the seasonal cycle of currents, temperature, stratification, and wind stress, *J. Phys. Oceanogr.*, **17**, 367–384, 1987.
- Chen, C., R. Beardsley, P. Franks, and J. Van Keuren, Influences of the diurnally varying heat flux on stratification and residual circulation on Georges Bank, *J. Geophys. Res.*, **108**(C11), 8008, doi:10.1029/2001JC001245, in press, 2003.
- Churchill, J. H., J. P. Manning, and R. C. Beardsley, Slope water intrusions onto Georges Bank, *J. Geophys. Res.*, **108**(C11), 8012, doi:10.1029/2002JC001400, in press, 2003.
- Cry, G. W., Tropical cyclones of the North Atlantic Ocean, *Tech. Rep. 55*, 149 pp., Weather Bureau, U.S. Dept. of Comm., Washington, D. C., 1965.
- Dean, J. P., and R. C. Beardsley, A vector-averaging wind recorder (VAWR) system for surface meteorological measurements in CODE, *Tech. Rep. WHOI-88-20*, 68 pp., Woods Hole Oceanogr. Inst., Woods Hole, Mass., 1988.
- Donelan, M. A., Air-sea Interaction, in *The Sea*, edited by B. LaMehaute and D. Hanes, pp. 239–292, John Wiley, Hoboken, N. J., 1990.
- Donelan, M. A., F. W. Dobson, S. D. Smith, and R. J. Anderson, On the dependence of sea surface roughness on wave development, *J. Phys. Oceanogr.*, **23**, 2143–2149, 1993.
- Fairall, C. W., E. F. Bradley, D. P. Rogers, J. B. Edson, and G. S. Young, Bulk parameterization air-sea fluxes for TOGA-COARE, *J. Geophys. Res.*, **101**, 3747–3764, 1996.
- Flagg, C. N., Hydrographic structure and variability, in *Georges Bank*, edited by R. H. Backus, pp. 108–124, MIT Press, Cambridge, Mass., 1987.
- Friehe, C. A., R. C. Beardsley, C. D. Winant, and J. P. Dean, Intercomparison of aircraft and surface buoy meteorological data during CODE-1, *J. Atmos. Oceanic Technol.*, **1**, 79–86, 1984.
- Hamilton, G. D., NOAA Data Buoy Office programs, *Bull. Am. Meteorol. Soc.*, **61**, 1012–1017, 1980.
- Hare, J. E., P. O. G. Persson, C. W. Fairall, and J. B. Edson, Behavior of Charnock's relationship for high wind conditions, paper presented at 13th Symposium of Boundary Layers and Turbulence, Am. Meteorol. Soc., Dallas, Tex., 1999.
- Hayden, B. P., and W. Smith, Season-to-season cyclone prediction, *Mon. Weather Rev.*, **110**, 239–253, 1982.
- Hopkins, T. S., and S. Raman, Atmospheric variables and patterns, in *Georges Bank*, edited by R. H. Backus, pp. 66–73, MIT Press, Cambridge, Mass., 1987.
- Hosom, D. S., R. A. Weller, R. E. Payne, and K. E. Prada, The IMET (Improved METeorology) ship and buoy systems, *J. Atmos. Oceanic Technol.*, **12**, 527–540, 1995.
- Johnson, H. K., J. Højstrup, H. J. Vested, and S. E. Larsen, On the dependence of sea surface roughness on wind waves, *J. Phys. Oceanogr.*, **28**, 1702–1716, 1998.
- Josey, S. A., A comparison of ECMWF, NCEP-NCAR, and SOC surface heat fluxes with moored buoy measurements in the subduction region of the Northeast Atlantic, *J. Clim.*, **14**, 1780–1789, 2001.
- Josey, S. A., E. C. Kent, and P. K. Taylor, The Southampton Oceanography Centre (SOC) Ocean-Atmosphere Heat, Momentum, and Freshwater Flux

- Atlas, *Rep. 6*, 30 pp., Southampton Oceanogr. Cent., Southampton, England, 1998.
- Kraus, E. B., and J. A. Businger, *Atmosphere-Ocean Interaction*, 362 pp., Oxford Univ. Press, New York, 1994.
- Large, W. G., and S. Pond, Open ocean momentum flux measurements in moderate to strong winds, *J. Phys. Oceanogr.*, *11*, 324–336, 1981.
- Lentz, S. J., R. C. Beardsley, J. D. Irish, J. Manning, P. C. Smith, and R. A. Weller, Temperature and salt balances on Georges Bank February–August 1995, *J. Geophys. Res.*, *108*(C11), 8006, doi:10.1029/2001JC001220, in press, 2003.
- MacWhorter, M. A., and R. A. Weller, Error in measurements of incoming shortwave radiation made from ships and buoys, *J. Atmos. Oceanic Tech.*, *8*, 108–117, 1991.
- Manning, J., and G. Strout, Georges Bank winds: 1975–1997, *Deep Sea Res. II*, *48*, 115–136, 2001.
- Mather, J., H. Adams, and G. Yoshioka, Coastal storms of the eastern United States, *J. Appl. Meteorol.*, *3*, 693–706, 1964.
- Miller, J. E., Cyclogenesis in the Atlantic coastal region of the United States, *J. Meteorol.*, *3*, 31–46, 1946.
- Mountain, D. G., G. A. Strout, and R. C. Beardsley, Surface heat flux in the Gulf of Maine, *Deep Sea Res. II*, *43*, 1533–1546, 1996.
- National Oceanic and Atmospheric Administration, Climatological Data, New England, August 1995, *107*(08), Silver Spring, Md., 1995a.
- National Oceanic and Atmospheric Administration, Climatological Data, Annual Summary, New England, 1995, *107*(13), Silver Spring, Md., 1995b.
- Pawlowicz, R., B. Beardsley, S. Lentz, E. Dever, and A. Anis, Software simplifies air-sea data estimates, *Eos Trans. AGU*, *84*, 2, 2001.
- Payne, R. E., Albedo of the sea surface, *J. Atmos. Sci.*, *29*, 959–970, 1972.
- Payne, R. E., Air temperature shield tests, *Tech. Rep. WHOI-87-40*, 22 pp., Woods Hole Oceanogr. Instit., Woods Hole, Mass., 1987.
- Serra, Y. L., P. A'Hearn, H. P. Freitag, and M. J. McPhaden, ATLAS self-siphoning rain gauge error estimates, *J. Atmos. Oceanic Technol.*, *18*, 1989–2002, 2001.
- Taylor, P. K., and M. J. Yelland, The dependence of sea surface roughness on the height and steepness of the waves, *J. Phys. Oceanogr.*, *31*, 2001.
- Weller, R. A., D. L. Rudnick, R. E. Payne, J. P. Dean, N. J. Pennington, and R. P. Trask, Measuring near-surface meteorology over the ocean from an array of surface moorings in the Subtropical Convergence Zone, *J. Atmos. Oceanic Technol.*, *7*, 86–103, 1990.
- Werner, S. R., R. C. Beardsley, S. J. Lentz, D. Hebert, and N. Oakey, Observations and modeling of the tidal bottom boundary layer on the southern flank of Georges Bank, *J. Geophys. Res.*, *108*(C11), 8005, doi:10.1029/2001JC001271, in press, 2003a.
- Werner, S. R., R. C. Beardsley, and A. J. Williams, Bottom friction and bedforms on the southern flank of Georges Bank, *J. Geophys. Res.*, *108*(C11), 8004, doi:10.1029/2000JC000692, in press, 2003b.
- Williams, J., *The Weather Book*, 212 pp., Vintage, New York, 1992.
- Yang, D., B. E. Goodison, J. R. Metcalfe, V. S. Golubev, R. Bates, T. Pangburn, and C. L. Hanson, Accuracy of NWS 8" standard non-recording precipitation gauge: Results and application of WMO inter-comparison, *J. Atmos. Oceanic Technol.*, *15*, 54–68, 1998.
- Yuter, S., and W. Parker, Rainfall measurement on ship revisited: The 1997 PACS TEPPS cruise, *J. Appl. Meteorol.*, *40*, 1003–1018, 2001.

R. C. Beardsley, J. B. Edson, J. D. Irish, S. J. Lentz, R. Limeburner, and R. A. Weller, Woods Hole Oceanographic Institution, Woods Hole, MA 02543, USA. (rbeardsley@whoi.edu; jedson@whoi.edu; jirish@whoi.edu; slentz@whoi.edu; rlimeburner@whoi.edu; rweller@whoi.edu)